Article

# Correlated C–C and C–O Bond Conformations in Saccharide Hydroxymethyl Groups: Parametrization and Application of Redundant H–H, C–H, and C–C NMR *J*-Couplings

Christophe Thibaudeau, Roland Stenutz, Brian Hertz, Thomas Klepach, Shikai Zhao, Qingquan Wu, Ian Carmichael, and Anthony S. Serianni

*J. Am. Chem. Soc.*, **2004**, 126 (48), 15668-15685• DOI: 10.1021/ja0306718 • Publication Date (Web): 11 November 2004



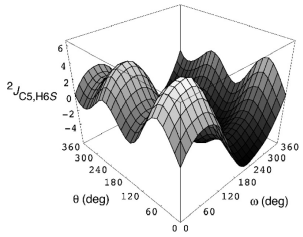


DFT-derived hypersurface showing the correlation between $^2J_{C5,H6S}$ and the C5-C6 (ω) and C6-O6 (θ) torsion angles in saccharides.

## More About This Article

Additional resources and features associated with this article are available within the HTML version:

- Supporting Information
- Links to the 5 articles that cite this article, as of the time of this article download
- Access to high resolution figures
- Links to articles and content related to this article
- Copyright permission to reproduce figures and/or text from this article

View the Full Text HTML

J|A|C|S
ARTICLES
Published on Web 11/11/2004

# Correlated C−C and C−O Bond Conformations in Saccharide Hydroxymethyl Groups: Parametrization and Application of Redundant $^1$H−$^1$H, $^{13}$C−$^1$H, and $^{13}$C−$^{13}$C NMR *J*-Couplings

Christophe Thibaudeau,[†] Roland Stenutz,[§] Brian Hertz,[†] Thomas Klepach,[†] Shikai Zhao,[||] Qingquan Wu,[†] Ian Carmichael,[‡] and Anthony S. Serianni*,[†]

*Contribution from the Department of Chemistry and Biochemistry and Radiation Laboratory, University of Notre Dame, Notre Dame, Indiana 46556-5670; Department of Organic Chemistry, Arrhenius Laboratory, Stockholm University, SE-106 91, Stockholm, Sweden; and Omicron Biochemicals, Inc., 1347 North Ironwood Drive, South Bend, Indiana 46615-3566*

Received December 18, 2003; E-mail: serianni.1@nd.edu

***Abstract:*** Methyl α- and β-pyranosides of D-glucose and D-galactose **1**−**4** were prepared containing single sites of $^{13}$C-enrichment at C4, C5, and C6 (12 compounds), and $^1$H and $^{13}$C{$^1$H} NMR spectra were obtained to determine a complete set of *J*-couplings ($^1J$, $^2J$, and $^3J$) involving the labeled carbon and nearby protons and carbons within the exocyclic hydroxymethyl group ($CH_2OH$) of each compound. In parallel theoretical studies, the dependencies of $^1J$, $^2J$, and $^3J$ involving $^1$H and $^{13}$C on the C5−C6 ($\omega$) and C6−O6 ($\theta$) torsion angles in aldohexopyranoside model compounds were computed using density functional theory (DFT) and a special basis set designed to reliably recover the Fermi contact contribution to the coupling. Complete hypersurfaces for $^1J_{C5,C6}$, $^2J_{C5,H6R}$, $^2J_{C5,H6S}$, $^2J_{C6,H5}$, $^2J_{C4,C6}$, $^3J_{C4,H6R}$, $^3J_{C4,H6S}$, and $^3J_{C6,H4}$, as well as $^2J_{H6R,H6S}$, $^3J_{H5,H6R}$, and $^3J_{H5,H6S}$, were obtained and used to parametrize new equations correlating these couplings to $\omega$ and/or $\theta$. DFT-computed couplings were also tested for accuracy by measuring *J*-couplings in $^{13}$C-labeled 4,6-*O*-ethylidene derivatives of D-glucose and D-galactose in which values of $\omega$ and $\theta$ were constrained. Using a new computer program, Chymesa, designed to utilize multiple *J*-couplings sensitive to exocyclic $CH_2OH$ conformation, the ensemble of experimental couplings observed in **1**−**4** were analyzed to yield preferred rotamer populations about $\omega$ and $\theta$. Importantly, due to the sensitivity of some couplings, most notably $^2J_{H6R,H6S}$, $^2J_{C5,H6R}$, and $^2J_{C5,H6S}$, to both $\omega$ and $\theta$, unique information on *correlated* conformation about both torsion angles was obtained. The latter treatment represents a means of evaluating correlated conformation in 1,6-linked oligosaccharides, since $\psi$ and $\theta$ are redundant in these linkages. In the latter regard, multiple, redundant scalar couplings originating from both sides of the glycosidic linkage can be used collectively to evaluate conformational correlations between $\psi/\theta$ and C5−C6 bond rotamers.

## Introduction

Conformational analysis of saccharides by NMR is often compromised by insufficient structural constraints on which to base firm conformational assignments.[1,2] This problem is particularly acute in studies of conformationally flexible domains, such as the exocyclic hydroxymethyl ($CH_2OH$) fragments of monosaccharides and the *O*-glycosidic linkages of oligo- and polysaccharides. In the former, the assignment of conformation is especially important when O6 is involved in the *O*-glycosidic linkage, since here three torsion angles define linkage geometry, namely, $\omega$, $\phi$, and $\psi$ (Scheme 1).

Experimental and theoretical studies of trans-*O*-glycoside couplings ($^2J_{COC}$, $^3J_{COCH}$, and $^3J_{COCC}$) were undertaken recently to determine their dependencies on oligosaccharide structure.[1−5] In addition to the expected Karplus dependence of $^3J_{COCC}$, terminal electronegative substituent effects were shown to be significant and quantifiable, leading to more accurate interpretations of these couplings in structural terms.[1,2] Likewise, $^3J_{HCCH}$, $^2J_{HCH}$, and $^1J_{CH}$ within saccharide exocyclic $CH_2OH$ groups were

***Scheme 1.*** Part of the Core Structure of Glycoprotein *N*-Glycans, Showing 1,3- and 1,6-Linkages and the $\psi/\theta$ Redundancy in the Latter

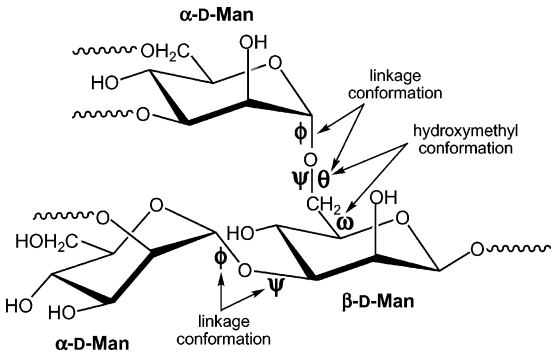


[†] Department of Chemistry and Biochemistry, University of Notre Dame.
[‡] Radiation Laboratory, University of Notre Dame.
[§] Stockholm University.
[||] Omicron Biochemicals, Inc.

(1) Bose, B.; Zhao, S.; Stenutz, R.; Cloran, F.; Bondo, P. B.; Bondo, G.; Hertz, B.; Carmichael, I.; Serianni, A. S. *J. Am. Chem. Soc.* **1998**, *120*, 11158−11173.
(2) Cloran, F.; Carmichael, I.; Serianni, A. S. *J. Am. Chem. Soc.* **1999**, *121*, 9843−9851.


**10.1021/ja0306718 CCC: $27.50** 

examined, leading to new equations correlating their magnitudes to $\omega$ and $\theta$ (Scheme 1).[6] These studies demonstrated that *J*-couplings often display dependencies on more than one molecular parameter. These secondary dependencies are useful when direct experimental parameters are either unavailable or inaccessible to probe a specific conformational feature. For example, prior work suggests that $^3J_{C1,C6}$ in aldohexopyranosyl rings not only display the expected Karplus dependence on the C1−O5−C5−C6 torsion angle but also respond predictably to changes in the O5−C5−C6−O6 torsion, suggesting that these couplings may be valuable indirect probes of hydroxymethyl group conformation.[1] *The two-parameter dependencies of J-couplings lead to the possibility of evaluating correlated conformations in saccharides.* To explore this potential, the present work aimed to identify the primary structural factor(s) governing specific *J*-couplings and to uncover and quantify secondary (and heretofore unknown) structural dependencies that may be exploited to assess correlated behaviors. We also attempted to identify the underlying structural features (e.g., bond lengths, bond angles, stereoelectronic effects) or trends that influence specific coupling magnitudes.

The above experimental aims are more compelling when considering the likelihood of conformational flexibility about $\omega$, $\phi$, and $\psi$ (Scheme 1). Arguments presented in the literature about whether oligosaccharides are rigid or flexible are largely moot; there is likely to be mobility about each of these bonds in solution. The key issues are the amplitudes and time scales of these motions, which are probably context-dependent.[5] Given the wide range of monosaccharides and the various modes of assembling them into oligomers, it will be challenging to establish whether these contexts can be systematically identified and categorized, thereby leading to reliable empirical rules correlating primary structure with oligosaccharide conformation and dynamics.

In this study, recent work[6] on *J*-couplings sensitive to saccharide exocyclic $CH_2OH$ conformation is extended. Previously we showed that density functional theory (DFT) calculations using a special basis set predict $^2J_{HH}$, $^3J_{HH}$, and $^1J_{CH}$ nearly quantitatively *without the need for scaling*, yielding new equations correlating these couplings with $\omega$ and/or $\theta$ (Scheme 1).[6] Herein, $^2J_{CH}$, $^3J_{CH}$, $^1J_{CC}$, $^2J_{CC}$, and $^3J_{CC}$ are examined experimentally and theoretically; additional data on $^2J_{HH}$ and $^3J_{HH}$ are also presented. Methyl D-gluco- and D-galactopyranoside anomers **1**−**4** were prepared singly $^{13}$C-enriched at C4, C5, and C6 and used for experimental determinations of $J_{CH}$ and $J_{CC}$ involving the carbons and hydrogens near the $CH_2OH$ substituent; these couplings include $^1J_{C5,C6}$, $^2J_{C5,H6R}$, $^2J_{C5,H6S}$, $^2J_{C6,H5}$, $^2J_{C4,C6}$, $^3J_{C4,H6R}$, $^3J_{C4,H6S}$, and $^3J_{C6,H4}$. Their interpretation was facilitated by DFT calculations in model structures **5**−**7** and by NMR measurements within conformationally constrained 4,6-*O*-ethylidene-D-gluco- and D-galactopyranoses. New parametrized equations relating $J_{HH}$, $J_{CH}$, and $J_{CC}$ to $\omega$ and/or $\theta$ have been developed, and a concerted analysis of multiple redundant *J*-couplings to evaluate correlated conformation about

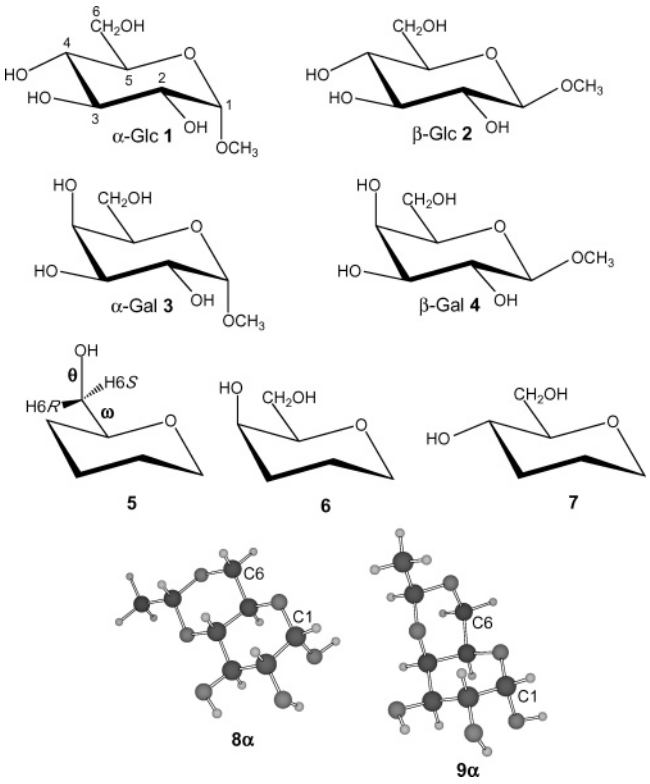


$\omega$ and $\theta$ in aldohexopyranosyl rings is described using a new computer program, Chymesa. The results have important implications for future investigations of biologically relevant oligosaccharides containing 1,6-glycosidic linkages.

## Experimental Section

**A. Synthesis of Labeled Methyl Aldohexopyranosides.** Methyl α-D-[4-$^{13}$C]-, [5-$^{13}$C]-, and [6-$^{13}$C]glucopyranosides (**1**); methyl $\beta$-D-[4-$^{13}$C]-, [5-$^{13}$C]-, and [6-$^{13}$C]glucopyranosides (**2**); methyl α-D-[4-$^{13}$C]-, [5-$^{13}$C]-, and [6-$^{13}$C]galactopyranosides (**3**); and methyl $\beta$-D-[4-$^{13}$C]-, [5-$^{13}$C]-, and [6-$^{13}$C]galactopyranosides (**4**) were prepared as described previously,[7,8] and only brief descriptions are provided here.

D-[4-$^{13}$C]Glucose and D-[5-$^{13}$C]glucose were prepared from DL-[1-$^{13}$C]- and [2-$^{13}$C]glyceraldehyde, respectively,[9] and dihydroxyacetone phosphate (DHAP)[10] using FBP aldolase (E.C. 4.1.2.13) (Scheme 2). The initially formed hexulose 1-phosphates were dephosphorylated with acid phosphatase (E.C. 3.1.3.2), and the neutral labeled D-fructose and L-sorbose were purified by chromatography on Dowex 50 × 8 (200−400 mesh) in the $Ca^{2+}$ form (fructose elutes first, followed by sorbose).[11] The purified labeled D-fructoses were treated with immobilized D-xylose isomerase (E.C. 5.3.1.5), and the resulting mixtures containing labeled D-glucoses and D-fructoses were purified by chromatography on Dowex 50 × 8 (200−400 mesh) in the $Ca^{2+}$ form (glucose elutes first, followed by fructose).

D-[6-$^{13}$C]Glucose was prepared from K$^{13}$CN and 1,2-*O*-isopropylidene-α-D-*xylo*-pentodialdo-1,4-furanose as described previously.[12] D-[4-$^{13}$C]-, [5-$^{13}$C]-, and [6-$^{13}$C]Galactoses were prepared from the corresponding labeled D-glucoses via C4-epimerization.[13]

(3) Church, T.; Carmichael, I.; Serianni, A. S. *Carbohydr. Res.* **1996**, *280*, 177−186.
(4) Serianni, A. S.; Bondo, P. B.; Zajicek, J. *J. Magn. Reson., Ser. B* **1996**, *112*, 69−74.
(5) Zhao, S.; Bondo, G.; Zajicek, J.; Serianni, A. S. *Carbohydr. Res.* **1998**, 309, 145−152.
(6) Stenutz, R.; Carmichael, I.; Widmalm, G.; Serianni, A. S. *J. Org. Chem.* **2002**, *67*, 949−958.
(7) Serianni, A. S.; Cadman, E.; Pierce, J.; Hayes, M. L.; Barker, R. *Methods Enzymol.* **1982**, *89*, 83−92.
(8) Serianni, A. S.; Vuorinen, T.; Bondo, P. *J. Carbohydr. Chem.* **1990**, *9*, 513−541.
(9) Serianni, A. S.; Clark, E. L.; Barker, R. *Carbohydr. Res.* **1979**, *72*, 79−91.
(10) Effenberger, F.; Straub, A. *Tetrahedron Lett.* **1987**, *28*, 1641−1644.
(11) Angyal, S. J.; Bethell, G. S.; Beveridge, R. J. *Carbohydr. Res.* **1979**, *73*, 9−18.
(12) King-Morris, M. J.; Bondo, P. B.; Mrowca, R. A.; Serianni, A. S. *Carbohydr. Res.* **1988**, *175*, 49−58.

*Scheme 2*

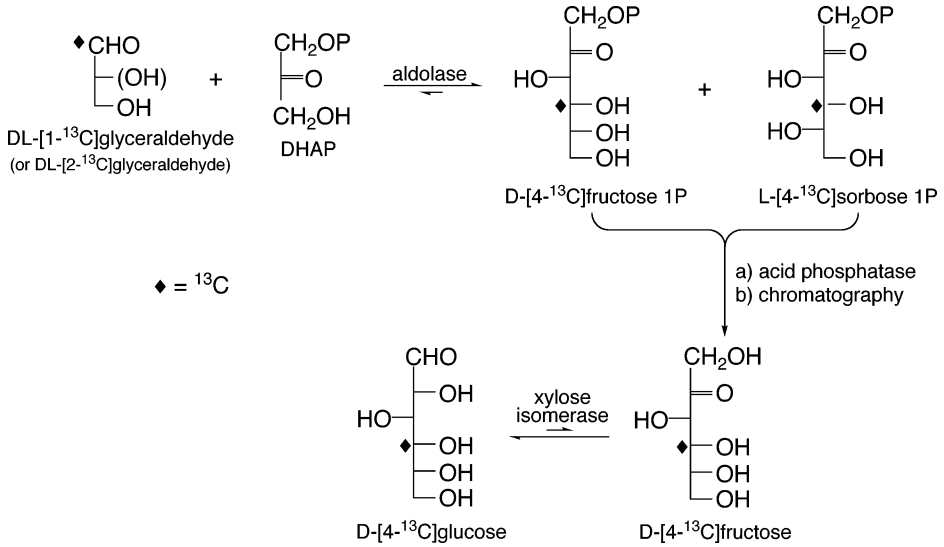


The labeled D-glucoses and D-galactoses were converted to their methyl pyranosides by treatment with anhydrous MeOH in the presence of Dowex 50 × 8 (20−50 mesh) resin in the $H^+$ form (Fischer glycosidation).[14] In each case, the mixture of anomeric aldohexopyranosides was purified by chromatography on Dowex 1 × 8 (200−400 mesh) ion-exchange resin in the $OH^-$ form, using water as the eluent.[15] Purified glycosides (12 total) were identified by their characteristic $^1H$ and $^{13}C$ chemical shifts.[14,16]

4,6-*O*-Ethylidene-D-[4-$^{13}$C]-, [5-$^{13}$C]-, and [6-$^{13}$C]glucoses, and 4,6-*O*-ethylidene-D-[6-$^{13}$C]galactose were prepared from the corresponding labeled D-hexoses as follows.[17] The labeled hexose (181 mg, 1.0 mmol) was mixed in a 10 mL round-bottom flask with acetaldehyde (60 $\mu$L, 1.1 mmol) and *p*-toluenesulfonic acid monohydrate (5 mg). The mixture was stirred at 5 °C overnight and extracted with hot ethyl acetate (3 × 8 mL), and the extract was concentrated at 30 °C in vacuo. The crude product was purified by chromatography on silica gel using MeOH/$CH_2Cl_2$ (7:1) as the solvent, and the derivatives were characterized by $^1H$ and $^{13}C$ NMR. Overall yields ranged from 15 to 25%; unreacted starting aldose, which accounted for the low yield, was recovered for reuse.

**B. NMR Spectroscopy.** $^1H$ and $^{13}C\{^1H\}$ NMR spectra of $^{13}C$-labeled methyl D-gluco- and D-galactopyranosides, and of $^{13}C$-labeled 4,6-*O*-ethylidene-D-gluco- and galactopyranoses, were obtained at 30 °C in $^2H_2O$ (∼50 m*M* for $^1H$; ∼200 m*M* for $^{13}C$) on a Varian Unity*Plus* FT-NMR spectrometer operating at 599.887 MHz for $^1H$ and 150.854 MHz for $^{13}C$. 1D Spectra were processed with optimal digital resolution and resolution enhancement to extract *J*-couplings having errors of ±0.1 Hz unless otherwise noted; couplings <0.5 Hz appeared as line-broadening. Spectral simulation was required to extract accurate $J_{HH}$ and $J_{CH}$ couplings in all cases and to determine/confirm coupling signs; MacNUTS[18] operating on Apple platforms was used to generate simulated $^1H$ NMR spectra.

**C. Theoretical Calculations.** The torsion angles, $\omega$ and $\theta$, are defined as O5−C5−C6−O6 and C5−C6−O6−O6H, respectively, in **1**−**7**. Density functional theory (DFT) calculations using the B3LYP functional[19] and the 6-31G* basis set[20] were conducted within *Gaussian*94[21] for geometric optimization of molecular structures.[1,2] Three model compounds (**5**−**7**) were used in the calculations. The most extensive data set was obtained on **5**, which lacks an OH substituent at C4, thus reducing complications caused by the arbitrary introduction of intramolecular hydrogen bonding (with concomitant undesirable changes in bond torsions) during the geometric optimizations. The $\omega$ and $\theta$ torsion angles in **5** were varied systematically from 0°−360° in 30° increments by holding both torsion angles at fixed values in the calculations, yielding 144 partially optimized geometries; all remaining molecular parameters were geometrically optimized. These data were used to generate the hypersurfaces. Nine structures were obtained containing staggered values of $\omega$ and $\theta$ wherein both torsion angles and all other degrees of freedom were optimized. A comparison of partially and fully optimized geometries gave an estimate of the extent to which holding $\omega$ and $\theta$ at fixed values affected the computed couplings.

A second series of calculations was performed on **6** and **7** that contain an axial and equatorial OH substituent at C4, respectively. In these calculations, one set of C−O torsion angles was inspected (C5−C4−O4−OH4 and C5−C6−O6−OH6 torsion angles of ∼180°), and only the three staggered rotamers about $\omega$ were studied (total of six structures). All structures were fully geometrically optimized. These calculations were performed to determine the effect of OH substituents on *J*-couplings involving C4 or H4 (e.g., $^3J_{C4,H6R/S}$, $^2J_{C5,H4}$, $^2J_{C4,C6}$). Restricting these calculations to a limited set of C−O torsions avoided complications caused by intramolecular H-bonding between O4 and O6 and their attached protons, which can distort geometries and induce undesirable torsion changes in the molecules.

A third series of calculations was performed on 4,6-*O*-ethylidene-α-D-glucopyranose (**8**α) and 4,6-*O*-ethylidene-α-D-galactopyranose (**9**α). As described for **6** and **7**, one set of C−O torsions was inspected (optimized torsions were as follows: for **8**α, C2−C1−O1−H = −172.0°, C1−C2−O2−H = −46.0°, C2−C3−O3−H = −48.2°; for **9**α, C2−C1−O1−H = −171.0°, C1−C2−O2−H = −44.3°, C2−C3−O3−H = −41.2°).

Coupling constants in **5**−**9** were calculated[2] by DFT using a modified version of *Gaussian*94[21] and an extended basis set ([5s2p1d|3s1p])[6]

(13) Zhao, S. Personal communication.
(14) Podlasek, C. A.; Wu, J.; Stripe, W. A.; Bondo, P.; Serianni, A. S. *J. Am. Chem. Soc.* **1995**, *117*, 8635−8644.
(15) Austin, P. W.; Hardy, F. E.; Buchanan, J. C.; Baddiley, J. *J. Chem. Soc.* **1963**, 5350−5353.
(16) Bock, K.; Pedersen, C. *Adv. Carbohydr. Chem. Biochem.* **1983**, *41*, 27−66.
(17) Bonner, T. G. *Methods Carbohydr. Chem.* **1963**, *2*, 309−313.
(18) *MacNUTs Pro*; Acorn NMR Inc.: Livermore, CA.
(19) Becke, A. D. *J. Chem. Phys.* **1993**, *98*, 5648−5652.
(20) Hehre, W. J.; Ditchfield, R.; Pople, J. A. *J. Chem. Phys.* **1972**, *56*, 2257−2261.
(21) Frisch, M. J.; Trucks, G. W.; Schlegel, H. B.; Gill, P. M. W.; Johnson, B. G.; Robb, M. A.; Cheeseman, J. R.; Keith, T.; Petersson, G. A.; Montgomery, J. A.; Raghavachari, K.; AlLaham, M. A.; Zakrzewski, V. G.; Ortiz, J. V.; Foresman, J. B.; Peng, C. Y.; Ayala, P. Y.; Chen, W.; Wong, M. W.; Andres, J. L.; Replogle, E. S.; Gomperts, R.; Martin, R. L.; Fox, D. J.; Binkley, J. S.; Defrees, D. J.; Baker, J.; Stewart, J. P.; Head-Gordon, M.; Gonzalez, C.; Pople, J. A. *Gaussian94*; Gaussian, Inc.: Pittsburgh, PA, 1995.

***Scheme 3.*** Idealized Staggered Rotamers ($\omega$) about the C5−C6 Bond of Aldohexopyranosyl Rings

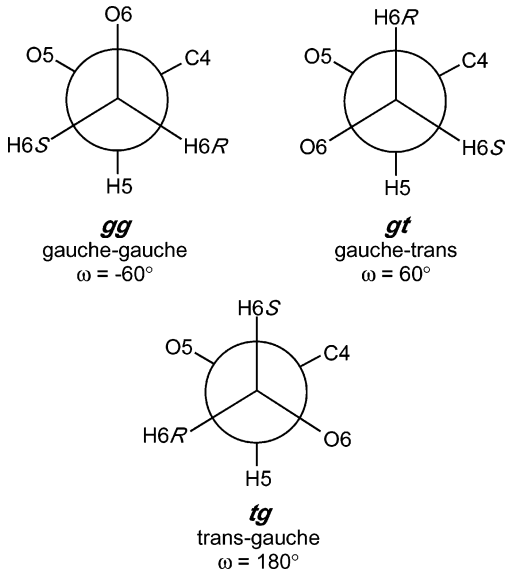


designed to reliably recover the Fermi contact contribution to the coupling. Prior work has shown that, in the present cases, contributions from the non-Fermi contact terms are small and can be neglected without significantly affecting the results. All computed couplings reported are *unscaled*, and all equations correlating structure with *J*-coupling magnitudes and signs were derived using unscaled couplings.

**D. Equation Parametrization.** Equations describing the dependencies of $^2J$ and $^3J$ on $\omega$ and $\theta$ were parametrized using ProFit 5.6.2 (Quantum Soft, Zürich, Switzerland). In the least-squares Monte Carlo fitting module integrated in ProFit, coefficients of the Fourier series used to formulate the equation were randomly generated, and for each set of coefficients, the deviation between *J*-values predicted by the equation and those from the reference dataset was calculated in the form of a $\chi^2$ parameter. In this work, the dataset consisted of 144 ($J$, $\omega$, $\theta$) points generated from the hypersurface calculations and of 9 freely optimized ($\omega$, $\theta$) rotamers. For each parametrized equation, $\chi^2$ was minimized in an iterative fashion. When no significant improvement in $\chi^2$ was observed compared to the "best" value, the calculation was terminated and the resulting set of coefficients was used to formulate the best fit equation.

Extended equations were parametrized to better describe the dependence of $J_{HH}$, $J_{CH}$, and $J_{CC}$ on $\omega$ and $\theta$ by systematically including $\omega$ or $\theta$ terms of increasing complexity in the Fourier series up to sin(2$x$) and cos(2$x$) and comparing the "best" $\chi^2$ values for each extended equation to the $\chi^2$ value generated by the simpler equations. In all cases, the number of terms was limited to 6 or 7 to avoid strongly correlated terms, which would produce an underdetermined system and an artificial improvement in $\chi^2$.

## Results and Discussion

**A. General Considerations.** Idealized staggered hydroxymethyl rotamers relevant to aldohexopyranosides are denoted *gg* ($\omega = -60°$), *gt* ($\omega = 60°$), and *tg* ($\omega = 180°$) (Scheme 3). The stereochemical assignments of H6*R* and H6*S* are shown in **5**, and rotamer definitions for $\theta$ are shown in Scheme 4.

Systematic rotations about $\omega$ and $\theta$ in **5** (30° increments) yielded 144 (12 × 12 matrix) structures that define a reasonable conformational energy hypersurface (Figure 1). Three energy minima are observed at the three staggered $\omega/\theta$ rotamers: 60°/−60° (0 kcal/mol); 300°/60° (0.4 kcal/mol); and 180°/−60° (2.9 kcal/mol). Thus, *gas-phase* DFT calculations at the B3LYP/6-31G* level of theory yielded the following relative stabilities

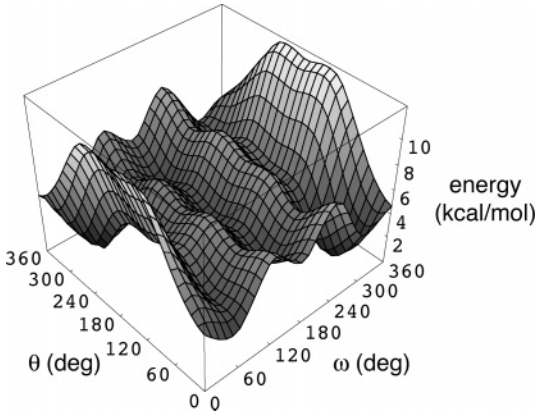


***Figure 1.*** Conformational energy hypersurface generated from 30° rotations of $\omega$ and $\theta$ in **5** (144 optimized structures) determined by DFT (B3LYP/6-31G*).

***Scheme 4.*** Idealized Staggered Rotamers ($\theta$) about the C6−O6 Bond of Aldohexopyranosyl Rings

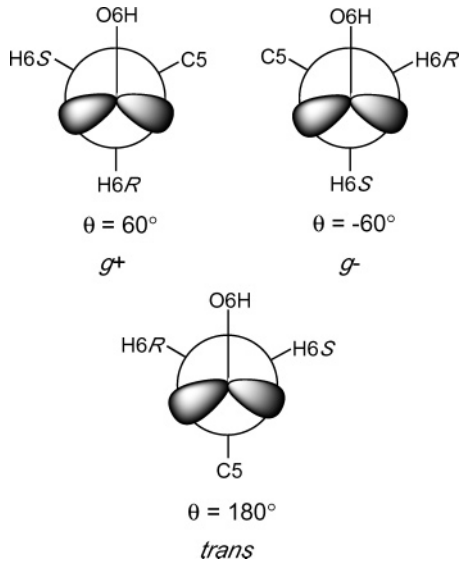


of hydroxymethyl rotamers in **5**: *gt* ≈ *gg* > *tg*. It should be noted, however, that the stabilities of the *gt* and *gg* rotamers may be affected by the location of O6H (i.e., by $\theta$); in *gg* and *gt*, O6H is oriented near one of the O5 lone pairs, and thus some stability may be conferred to both geometries due to intramolecular H-bonding. Indeed, *gg* and *gt* were *higher* in energy than *tg* when $\theta$ in the former was rotated to eliminate this H-bonding. Thus, *in the absence of solvent*, *tg* may be more stable than *gg* and *gt* when contributions from intramolecular H-bonding are eliminated, despite the presence of the gauche effect[22] in the latter forms which has been invoked to explain the experimentally determined preference for *gg* and *gt* in aqueous solution.

Introduction of an OH group at C4 of **5**, giving **6** or **7**, affects the relative stabilities of rotamers. For **6**, *tg* (0.1 kcal/mol) > *gt* (1.5 kcal/mol) ≫ *gg* (6.5 kcal/mol); for **7**, *gg* (0 kcal/mol) ≈ *gt* (0.4 kcal/mol) > *tg* (2.6 kcal/mol). These trends contrast with that observed for **5**, where *tg* (0 kcal/mol) > *gt* (1.4 kcal/mol) ≈ *gg* (1.9 kcal/mol) *for* $\theta = 180°$. The presence of an axial O4

(22) (a) Wolfe, S. *Acc. Chem. Res.* **1972**, *5*, 102−111. (b) Wiberg, K. B.; Murcko, M. A.; Laidig, K. E.; MacDougall, P. J. *J. Phys. Chem.* **1990**, *94*, 6956−6959. (c) Zefirov, N. S.; Samoshin, V. V.; Subbotin, O. A.; Baranenkov, V. I.; Wolfe, S. *Tetrahedron* **1978**, *34*, 2953−2959.

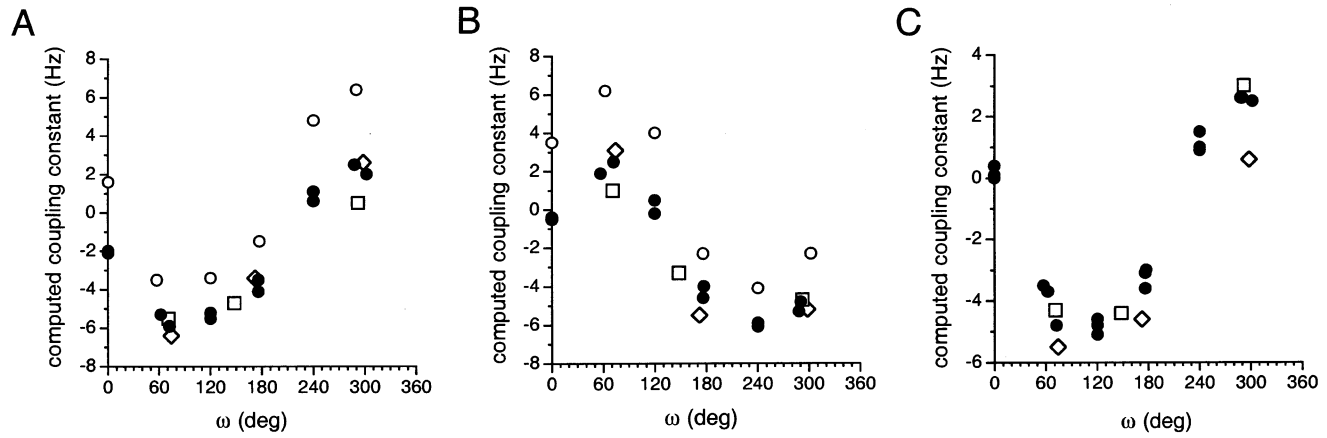


***Figure 2.*** (A) Dependence of $^2J_{C5,H6R}$ on $\omega$. (B) Dependence of $^2J_{C5,H6S}$ on $\omega$. (C) Dependence of $^2J_{C6,H5}$ on $\omega$. Circles, data from **5** (Table 1); open diamonds, data from **6** (Table S1); open squares, data from **7** (Table S1). For **5** in plots A and B, data are divided into two groups to emphasize the enhanced coupling (open circles) observed in one $\theta$ conformation (see Scheme 5).

(**6**) destabilizes *gg* but exerts a minimal effect on the *relative* energies of *gt* and *tg*. Introduction of an equatorial O4 stabilizes *gg* and *gt* significantly and destabilizes *tg*. However, results for **6** and **7** pertain to a small subset of C−O rotamers where intramolecular hydrogen bonding is weak or nonexistent, and relative populations derived from *gas-phase* calculations are expected to change significantly when the remaining C−O rotamers are taken into account, due to selective H-bonding in some forms. For these reasons, relying on conformational energy maps to predict preferences about $\omega$ can be problematic, since H-bonding and solvation forces affect torsional preferences.

**B. Calculated NMR Scalar Coupling Constants and Parametrization. 1. Two-Bond $^{13}$C−$^1$H Spin−Spin Coupling Constants.** $^2J_{CH}$ Values are useful structural constraints in saccharides, nucleosides and their derivatives,[6,14,23] and general rules have been proposed relating $^2J_{CCH}$ to specific patterns of oxygen atom substitution on the coupled carbon and on the carbon bearing the coupled hydrogen.[23a−c] With respect to $CH_2$-OH conformation, three $^2J_{CCH}$ are expected to be sensitive to $\omega$: $^2J_{C5,H6R}$, $^2J_{C5,H6S}$, and $^2J_{C6,H5}$. Computed values of these couplings in **5** are given in Table 1. Application of the projection rule[23a] yields two projections, 0 and 1.5, that correlate with average DFT-calculated $^2J_{CCH}$ values of $-3.8 \pm 1.2$ Hz and $+3.2 \pm 1.8$ Hz, respectively, using data in Table 1. As noted previously,[24,25] these computed couplings are shifted to more negative values than predicted by the projection rule.

The dependencies of $^2J_{CCH}$ on $\omega$ and $\theta$ are shown in Figure 2 for eclipsed and staggered $\omega$ rotamers. A single maximum and a single minimum are observed upon sampling $\omega$ from 0° to 360°. This behavior differs from that exhibited by $^3J_{CH}$ and $^3J_{HH}$ (see below), which display two maxima and two minima, and suggests a practical advantage of $^2J_{CH}$ in studies of $CH_2$-OH conformation, namely, greater reliability in correlating experimental couplings to rotamer populations due to the smaller number of conformers compatible with extreme and intermediate experimental couplings. The dynamic range of $^2J_{CCH}$ is $\sim+5$ Hz to $\sim -5$ Hz ($\Delta \approx 10$ Hz), which is comparable to, if not slightly larger than, that observed for $^3J_{CCCH}$ ($\Delta \approx 8$ Hz) (see below). The signs of $^2J_{CH}$ depend on $\omega$ and are straightforward to determine experimentally.[26] Note that plots of $^2J_{C5,H6R}$ and $^2J_{C5,H6S}$ in Figure 2 are complementary, which is a useful feature for stereochemical assignments of H6*R* and H6*S* and for $CH_2$-OH conformational analysis.

$^2J_{C5,H6R}$ and $^2J_{C5,H6S}$ exhibit a dependence on $\theta$ similar to that observed for $^2J_{H6R,H6S}$.[6] Two groups of couplings are observed at a given $\omega$ for the three staggered $\theta$ rotamers (Figure 2A,B); two couplings are similar in magnitude and always smaller (more negative) than the third. The $\theta$ rotamer in which OH6 is gauche to both coupled nuclei consistently exhibits a more *positive* coupling than the remaining two staggered rotamers (Scheme 5). The effect is enhanced when the coupled proton is

***Table 1.*** Torsion Angles[a], $\omega$ and $\theta$, and Calculated $^2J_{CH}$ Values[b] in **5**

| $\omega$[c] | $\theta$[d] | $^2J_{C5,H6R}$ | $^2J_{C5,H6S}$ | $^2J_{C6,H5}$ | C5–C6 rotamer[e] |
|---|---|---|---|---|---|
| 62 | 57 | −5.3 | +6.2 | −3.7 | |
| 57 | −48 | −3.5 | +1.9 | −3.5 | *gt* |
| 72 | 192 | −5.9 | +2.5 | −4.8 | |
| −58 | 50 | +2.0 | −2.3 | +2.5 | |
| −70 | −72 | +6.4 | −4.8 | +2.6 | *gg* |
| −72 | 171 | +2.5 | −5.3 | +2.6 | |
| 176 | 74 | −3.5 | −2.3 | −3.1 | |
| 177 | −69 | −1.5 | −4.0 | −3.0 | *tg* |
| 176 | 176 | −4.1 | −4.6 | −3.6 | |
| 120 | 60 | −5.5 | +4.0 | −4.8 | |
| 120 | −60 | −3.4 | +0.5 | −4.6 | |
| 120 | 180 | −5.2 | −0.2 | −5.1 | |
| 0 | 60 | −2.0 | +3.5 | +0.4 | |
| 0 | −60 | +1.6 | −0.4 | 0.0 | |
| 0 | 180 | −2.0 | −0.4 | +0.1 | |
| −120 | 60 | +1.1 | −4.1 | +0.9 | |
| −120 | −60 | +4.8 | −6.1 | +1.5 | |
| −120 | 180 | +0.6 | −5.9 | +1.0 | |

[a] In degrees. [b] In Hz. [c] Defined as O5−C5−C6−O6. [d] Defined as C5−C6−O6−HO6. [e] Defined in Scheme 3.

(23) (a) Bock, K.; Pedersen, C. *Acta Chem. Scand., Ser. B* **1977**, *B31*, 354−358. (b) Schwarcz, J. A.; Perlin, A. S. *Can. J. Chem.* **1972**, *50*, 3667−3676. (c) Schwarcz, J. A.; Cyr, N.; Perlin, A. S. *Can. J. Chem.* **1975**, *53*, 1872−1875. (d) Bandyopadhyay, T.; Wu, J.; Stripe, W. A.; Carmichael, I.; Serianni, A. S. *J. Am. Chem. Soc.* **1997**, *119*, 1737−1744. (e) Bandyopadhyay, T.; Wu, J.; Serianni, A. S. *J. Org. Chem.* **1993**, *58*, 5513−5517. (f) Church, T. J.; Carmichael, I.; Serianni, A. S. *J. Am. Chem. Soc.* **1997**, *119*, 8946−8964.
(24) Cloran, F.; Carmichael, I.; Serianni, A. S. *J. Phys. Chem. A* **1999**, *103*, 3783−3795.
(25) Cloran, F.; Carmichael, I.; Serianni, A. S. *J. Am. Chem. Soc.* **2001**, *123*, 4781−4791.
(26) (a) Serianni, A. S.; Podlasek, C. A. *Carbohydr. Res.* **1994**, *259*, 277−282. (b) Marino, J. P.; Schwalbe, H.; Glaser, S. J.; Griesinger, C. *J. Am. Chem. Soc.* **1996**, *118*, 4388−4395.

***Scheme 5.*** $\theta$ Rotamers that Make a Positive Contribution to $^2J_{C5,H6R}$ (A), $^2J_{C5,H6S}$ (B), and $^2J_{H6R,H6S}$ (C)[a]

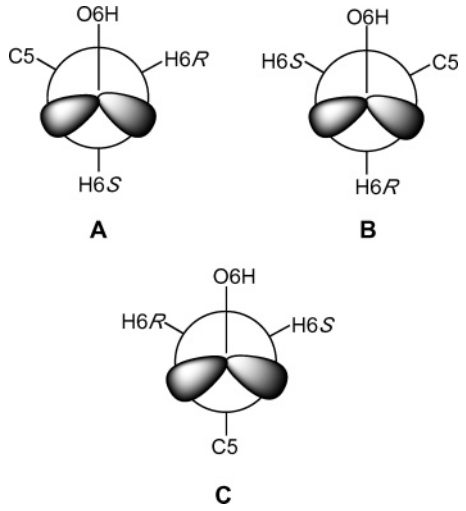


[a] In each case, the O6−O6H bond bisects the bond angle between the coupled nuclei.

anti to O5 (an increase of ∼+4 Hz vs ∼+2.3 Hz). This observation is consistent with that made for $^2J_{H6R,H6S}$ where $\theta$ having OH6 gauche to H6*R* and H6*S* contributes positively to the coupling (Scheme 5C). The origin of this effect remains unclear, although it is noted that, in all three geometries, both coupled atoms are anti to an O6 lone pair. The expected C−H and C−C bond elongation[27] may be partly responsible for the shift to more positive couplings. This effect is not observed for $^2J_{C6,H5}$ (Figure 2C), presumably because the C5−O5 torsion is held relatively fixed by the pyranosyl ring and cannot modulate the coupling.

Substitution of an OH group at C4 appears to affect $^2J_{C5,H6R}$ and $^2J_{C5,H6S}$ in those ring geometries in which the coupled proton experiences a 1,3-interaction with O4. In these cases, the coupling is shifted to a more negative value. For example, $^2J_{C5,H6S}$ is shifted to a more negative (less positive) value in **7** (by ∼2 Hz) compared to **6** for $\omega = +60°$ (Table S1); in the *gt* rotamer, H6*S* experiences a 1,3-interaction with the equatorial O4 in **7** which is absent in **6**. Essentially no effect of O4 is observed in the *gg* rotamer (when differences in $\omega$ are accounted for) regardless of C4 configuration, presumably because H6*S* is anti to C4 and thus well removed from the site of substitution. The above-noted 1,3-factor may be caused by small changes in C−H bond length induced by O4 lone pair effects; in this case, the oxygen lone pairs are expected to reduce bond lengths slightly,[27] which may lead to the slightly more negative $^2J_{CH}$.

An effect of C4 hydroxylation on $^2J_{C6,H5}$ is also observed, but only when O4 is axial (Figure 2C). The coupling is shifted to a more *negative* value in the three staggered $\omega$ rotamers. This observation is consistent with prior reports of "remote" effects on $^2J_{CCH}$ in aldohexopyranosides;[14] oxygen substituents trans to the coupled proton on adjacent carbons shift $^2J_{CCH}$ to more negative values (Scheme 6). The effect appears additive in that the shift observed in *gg* is ∼2-fold greater than that observed in *gt*, due to the presence of two anti oxygens (O4 and O6) in the former.

***Scheme 6***

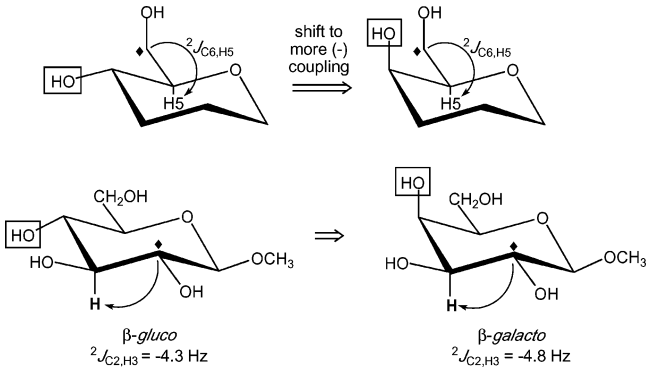


The above discussion reveals a significant effect of C−O bond torsions on $^2J_{CCH}$ magnitudes which were anticipated earlier.[6] To explore this effect further, a full hypersurface was obtained for **5** wherein $\omega$ and $\theta$ were sampled in 30° increments from 0° to 360°. Two-dimensional plots for $^2J_{C5,H6R}$, $^2J_{C5,H6S}$, and $^2J_{C6,H5}$ are shown in Figure 3A and B. Superimposed on these plots are computed couplings determined in nine fully optimized structures (Table 1). The latter data agree with those obtained from partially optimized geometries, *indicating that fixing $\omega$ and $\theta$ does not significantly alter the computed couplings*. These results show that the effect of $\theta$ on $^2J_{CCH}$ is greater when the carbon bearing the oxygen *also bears the coupled proton*, as opposed to the coupled carbon; rotating $\theta$ exerts a greater effect on $^2J_{C5,H6R}$ and $^2J_{C5,H6S}$ than on $^2J_{C6,H5}$, as revealed by the narrower range of couplings observed for the latter at discrete values of $\omega$. This effect is more clearly observed in the 3D hypersurfaces shown in Figures 3C−E. Presumably vicinal O6 lone pair effects[28] on the C6−H6*R*/*S* bond lengths (see below) perturb $^2J_{C5,H6R/S}$ more than O6 vicinal lone pair effects on the C5−C6 bond length perturb $^2J_{C6,H5}$. For this reason, $^2J_{C6,H5}$ may be more attractive than $^2J_{C5,H6R}$ and $^2J_{C5,H6S}$ for studies of $CH_2OH$ conformation when information about $\theta$ is unavailable. In addition, the *range* of allowed couplings at each value of $\omega$ is essentially the same as that shown in Figure 2 when only staggered $\theta$ values were considered. The latter fact leads to simplified equations relating these couplings to $\omega$ and $\theta$, as described below.

Valence bond angle, which has been shown to affect $^2J_{HCH}$,[29] might also influence $^2J_{CCH}$ values. However, in the fully optimized, staggered structures reported in Table 1, the C−C−H bond angle does not vary significantly; the average C5−C6−H6*R*, C5−C6−H6*S*, and C6−C5−H5 bond angles (±1 SD) are 108.8° ± 0.5°, 108.8° ± 0.6°, and 108.1° ± 0.8°, respectively. This distribution compares favorably with that found previously for the H6*R*−C6−H6*S* bond angle (107.7° ± 0.4°),[6] indicating that the C−C−H bond angle is probably not responsible for the observed dependence of $^2J_{CCH}$ on $\omega$ and $\theta$, at least within the group of structures studied.

The dependencies of $^2J_{C5,H6R}$ and $^2J_{C5,H6S}$ on $\omega$ and $\theta$ were parametrized using the complete dataset of 153 datapoints (144 structures from the hypersurface; 9 staggered structures in Table 1), yielding eqs 1a and b. Equation 1c describes the dependence of $^2J_{C6,H5}$ on $\omega$; attempts to parametrize this equation by

(27) Cloran, F.; Zhu, Y.; Osborn, J.; Carmichael, I.; Serianni, A. S. *J. Am. Chem. Soc.* **2000**, *122*, 6435−6448.
(28) Serianni, A. S.; Wu, J.; Carmichael, I. *J. Am. Chem. Soc.* **1995**, *117*, 8645−8650.
(29) Maciel, G. E.; McIver, J. W.; Ostlund, N. S.; Pople, J. A. *J. Am. Chem. Soc.* **1970**, *92*, 4151− 4157.

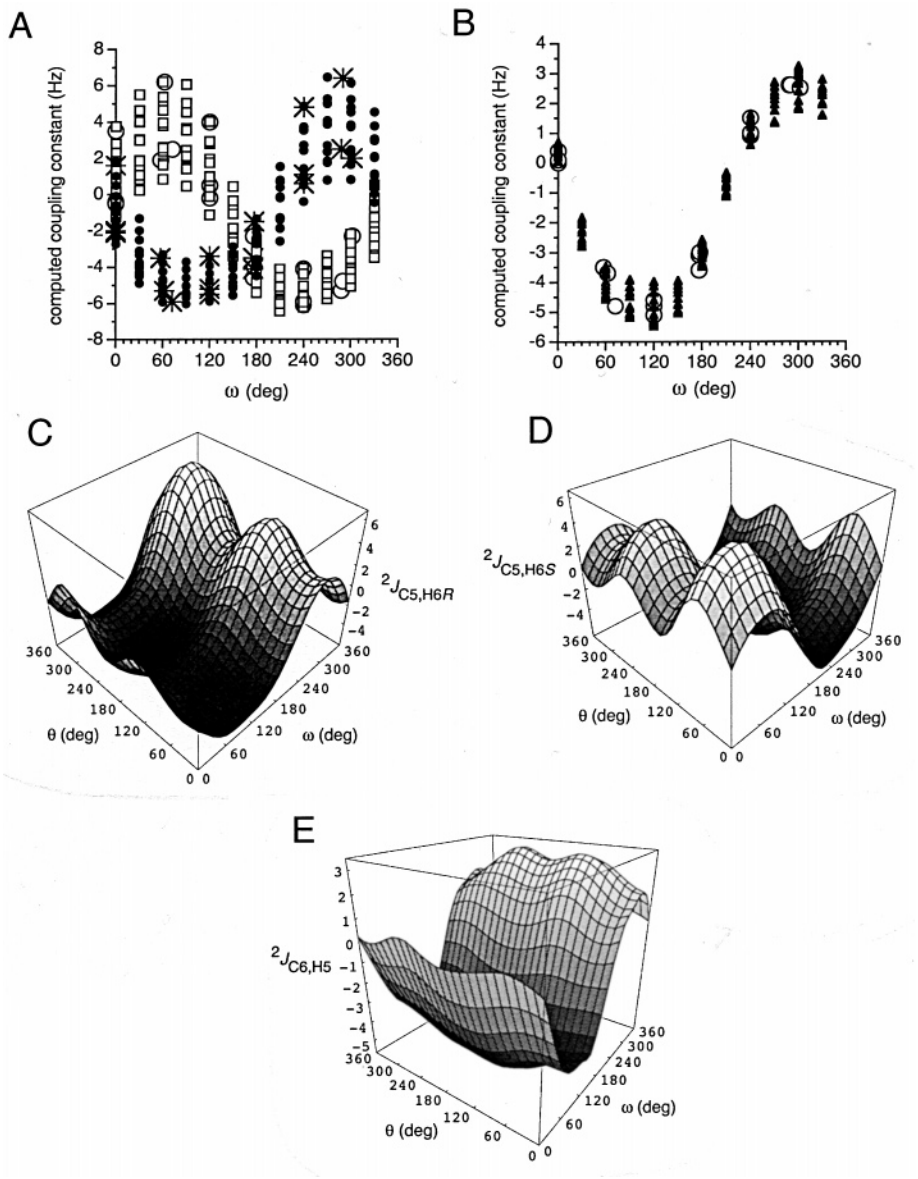


***Figure 3.*** (A) The dependence of $^2J_{C5,H6R/S}$ on both $\omega$ and $\theta$, determined by varying both torsion angles in **5** systematically through 360° in 30° increments. The vertical spread of points at discrete $\omega$ values demonstrates the sensitivity of these $^2J_{CH}$ to $\theta$. Superimposed are coupling data computed in the fully (staggered) and partially (eclipsed) optimized structures reported in Table 1. Filled circles, $^2J_{C5,H6R}$; open squares, $^2J_{C5,H6S}$; stars and open circles, respective couplings taken from Table 1. (B) Data similar to that in part A for $^2J_{C6,H5}$ in **5**. Closed triangles, hypersurface data; open circles, data from Table 1. (C) Hypersurface ($\omega/\theta$) calculated for $^2J_{C5,H6R}$ in **5**. (D) Hypersurface ($\omega/\theta$) calculated for $^2J_{C5,H6S}$ in **5**. (E) Hypersurface ($\omega/\theta$) calculated for $^2J_{C6,H5}$ in **5**.

including both $\omega$ and $\theta$ terms did not improve the rms error significantly.

$$^2J_{C5,H6R} = -1.40 + 0.94\cos(\omega) - 4.38\sin(\omega) - 0.79\cos(2\theta) - 1.24\sin(2\theta) \quad (\text{rms} = 0.78\ \text{Hz}) \quad (1a)$$

$$^2J_{C5,H6S} = -1.32 + 2.24\cos(\omega) + 4.12\sin(\omega) - 0.80\cos(2\theta) + 1.24\sin(2\theta) \quad (\text{rms} = 0.70\ \text{Hz}) \quad (1b)$$

$$^2J_{C6,H5} = -1.29 + 1.53\cos(\omega) - 3.68\sin(\omega) \quad (\text{rms} = 0.45\ \text{Hz}) \quad (1c)$$

**2. Three-Bond $^{13}$C−$^1$H Spin−Spin Coupling Constants.** $^3J_{C4,H6R}$ and $^3J_{C4,H6S}$ have been used previously to make stereochemical signal assignments of H6*R* and H6*S* in $^1$H NMR spectra of aldohexopyranosyl rings, and in studies of $CH_2OH$ conformation.[14,30,31] A Karplus relationship has been reported[31] and was applied recently to interpret $^3J_{C4,H6R}$ and $^3J_{C4,H6S}$ in aldohexopyranosyl rings.[32]

Theoretical relationships among $^3J_{C4,H6R}$, $^3J_{C4,H6S}$, $\omega$, and $\theta$ were examined initially in **5** using fully and partially geometrically optimized structures (Table S2). These data are plotted in Figure 4A, with the C−C−C−H torsion angle $\phi$ represented on the *x*-axis rather than $\omega$. The distribution of data points at discrete values of $\phi$ reveals the sensitivity of $^3J_{CCCH}$ to $\theta$. In comparison to $^2J_{CCH}$ (see above), the effect of $\theta$ on $^3J_{CCCH}$ is much reduced, as illustrated in the 3D hypersurfaces (Figure 4B and C) (note that the effect of C4−O4 bond rotation

(30) (a) Hayes, M. L.; Serianni, A. S.; Barker, R. *Carbohydr. Res.* **1982**, *100*, 87−101. (b) Morat, C.; Taravel, F. R.; Vignon, M. R. *Magn. Reson. Chem.* **1988**, *26*, 264−270. (c) Poppe, L.; Struike-Prill, R.; Meyer, B.; van Halbeek, H. *J. Biomol. NMR* **1992**, *2*, 109−136. (d) Poppe, L. *J. Am. Chem. Soc.* **1993**, *115*, 8421−8426.
(31) Tvaroska, I.; Gadjos, J. *Carbohydr. Res.* **1995**, *271*, 151−162.
(32) Tvaroska, I.; Taravel, F. R.; Utille, J. P.; Carver, J. P. *Carbohydr. Res.* **2002**, *337*, 353−367.

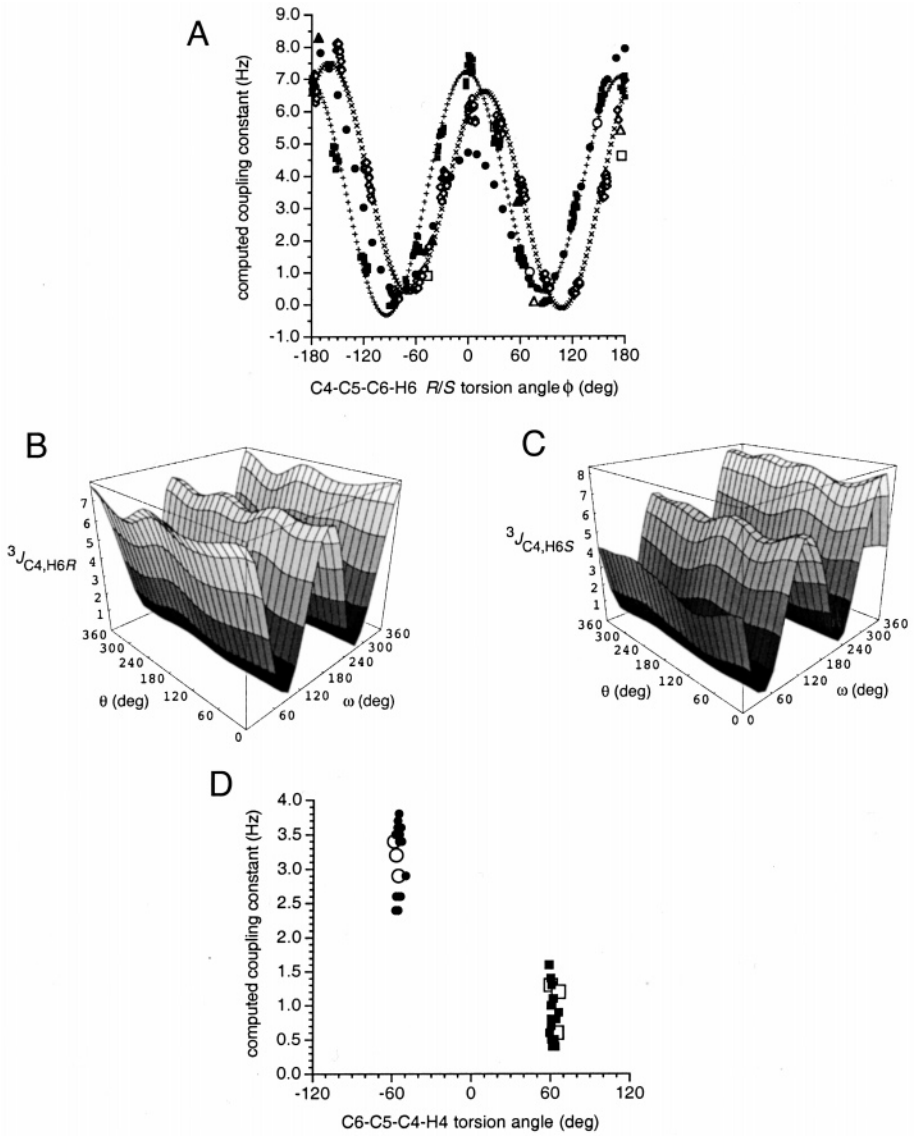


***Figure 4.*** (A) Dependence of $^3J_{C4,H6R}$ and $^3J_{C4,H6S}$ on $\phi$ in **5**. Filled squares, $^3J_{C4,H6R}$ (hypersurface data); open diamonds, $^3J_{C4,H6S}$ (hypersurface data); filled circles, $^3J_{C4,H6R/S}$ curve reported by Tvaroska and Gadjos;[31] open triangles, $^3J_{C4,H6R}$ in **6**; filled triangles, $^3J_{C4,H6S}$ in **6**; open circles, $^3J_{C4,H6R}$ in **7**; open squares, $^3J_{C4,H6S}$ in **7**. Small black + ($^3J_{C4,H6R}$) and X ($^3J_{C4,H6S}$) define Karplus curves predicted from eqs 2 and 3. The vertical spread of points at discrete $\phi$ indicates the effect of $\theta$. (B) Hypersurface calculated for $^3J_{C4,H6R}$ in **5**. (C) Hypersurface calculated for $^3J_{C4,H6S}$ in **5**. (D) Dependence of $^3J_{C6,H4}$ in **5** on the C6−C5−C4−H4 torsion angle (Table S2). Filled circles, $^3J_{C6,H4ax}$; filled squares, $^3J_{C6,H4eq}$. The vertical spread of points at discrete C−C−C−H torsions shows the effect of $\theta$. Data for corresponding couplings in **6** (open squares) and **7** (open circles) are also shown.

on $^3J_{C4,H6R/S}$ was not evaluated, but this effect is expected to be small based on observations made above on $^2J_{CCH}$). Both $^3J_{C4,H6R}$ and $^3J_{C4,H6S}$ display a Karplus dependence as expected, but the two curves are phase-shifted by ∼20°. For comparison, the previously reported theoretical curve[31,32] is shown in Figure 4A. While the general features of both treatments are conserved, predicted couplings for $\phi \pm 30°$ differ significantly, with larger values predicted by the present treatment.

Concern about the applicability of Karplus curves derived from theoretical studies of **5** to the analysis of experimental couplings observed in authentic aldohexopyranosyl rings substituted with oxygen on C4 (i.e., **1**−**4**) was addressed by calculating $^3J_{CCCH}$ in **6** and **7** (Figure 4A). Although the data for **6** and **7** are limited, there is no indication that O4 substitution significantly alters the relationships; ∼1 Hz deviations are observed at $\phi \approx 180°$ for both couplings, whereas differences at $\phi = \sim 60°$ and $-60°$ are insignificant. The small phase shift is also evident in the limited data obtained on **6** and **7**. We conclude that two different equations are required to describe the structural dependencies of $^3J_{C4,H6R}$ and $^3J_{C4,H6S}$ and that the curves derived from **5** are applicable, to a first approximation, to rings bearing OH substituents at C4.

Data in Table S2 yield additional insight into the effect of oxygen substituents on $^3J_{CCCH}$. $^3J_{C4,H6R}$ in the *gg* and *gt* rotamers is 1.1 ± 0.6 Hz and 1.2 ± 0.6 Hz for $\phi$ of −66.1° ± 8.8° and 64.8° ± 8.6°, respectively. $^3J_{C4,H6S}$ in *gt* and *tg* rotamers is 1.1 ± 0.7 Hz and 3.7 ± 0.2 Hz, respectively, for $\phi$ of −52.6° ± 9.2° and 59.8° ± 3.2°, respectively. Thus, the larger gauche coupling observed for $^3J_{C4,H6S}$ in *tg* is not caused by a significantly reduced $\phi$. This behavior is attributed to anti electronegative substituent effects caused by O5 and O6. For $^3J_{C4,H6S}$ in *tg*, O5 is gauche to H6*S*, and O6 is gauche to C4 (i.e., there are no electronegative substituents anti to either coupled nuclei). In contrast, there is at least one electronegative

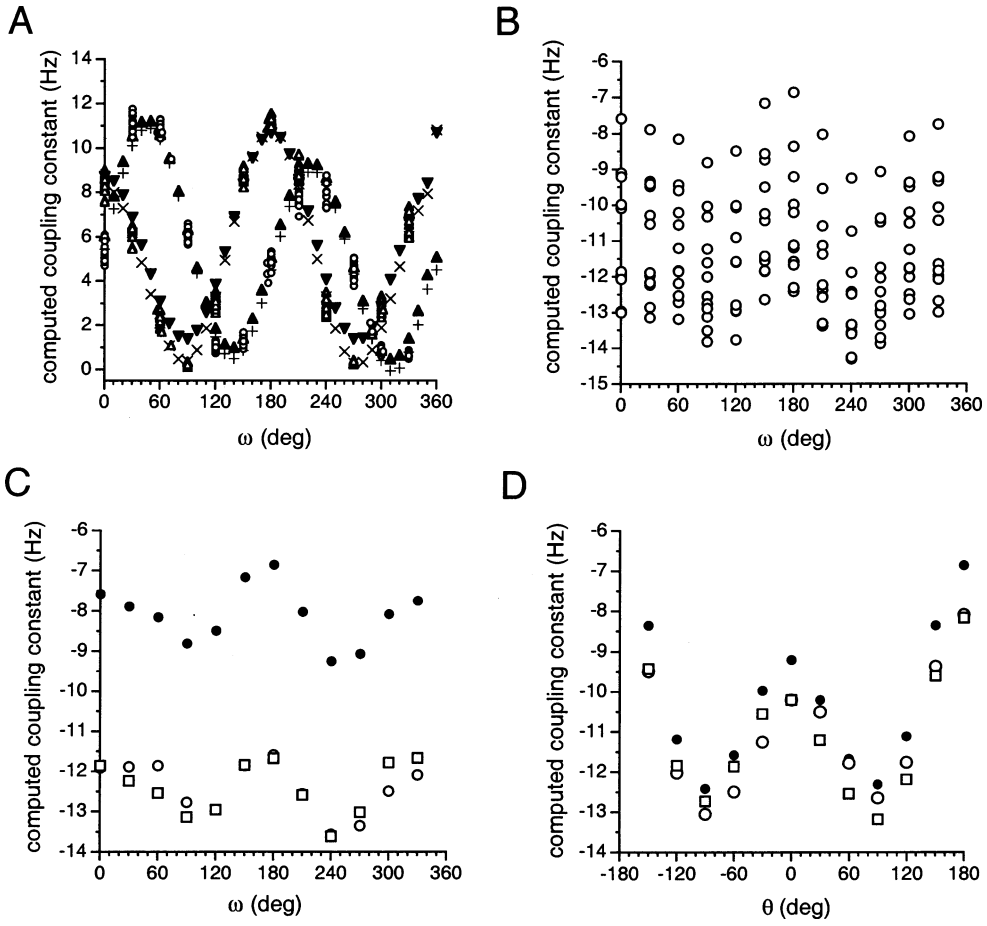


***Figure 5.*** (A) Dependence of $^3J_{H5,H6R}$ and $^3J_{H5,H6S}$ on $\omega$ in **5** (open circles, $^3J_{H5,H6R}$; open triangles, $^3J_{H5,H6S}$). The vertical spread of points at discrete $\omega$ torsions indicates the effect of $\theta$. Curves derived from eqs 4 and 5 (+ and ×), and curves derived from previously reported empirically derived Karplus equations[33] (filled upright and inverted triangles) are also shown. (B) Dependence of $^2J_{H6R,H6S}$ on $\omega$ in **5**. The vertical spread of points at discrete C−C−C−H torsions indicates the effect of $\theta$. (C) The dependence of $^2J_{H6R,H6S}$ in **5** on $\omega$ in the three perfectly staggered $\theta$ rotamers (open squares, $\theta = 60°$; open circles, $\theta = -60°$; filled circles, $\theta = 180°$). (D) Dependence of $^2J_{H6R,H6S}$ in **5** on $\theta$ in the three perfectly staggered $\omega$ rotamers (open squares, $\omega = 60°$; open circles, $\omega = -60°$; filled circles, $\omega = 180°$).

substituent anti to a coupled nucleus in the remaining three cases. For example, for $^3J_{C4,H6S}$ in *gt*, H6*S* is anti to O5, and O6 is anti to C4, whereas for $^3J_{C4,H6R}$ in *gg* and *gt*, only one anti interaction is present. It appears that this "anti" effect, which is related to that reported for $^3J_{HH}$,[6] is not additive; the presence of one of these interactions appears sufficient to reduce a gauche C−C−C−H coupling to its minimum value. The observed decrease in $^3J_{CCCH}$ upon introduction of one "anti" interaction is ~2.6 Hz.

Karplus dependencies for $^3J_{C4,H6R}$ and $^3J_{C4,H6S}$ using 18 datapoints (i.e., 9 staggered and 9 eclipsed $\omega$ conformers in Table S2) are described by eqs 2 and 3 in which $\omega$ is used (instead of $\phi$ shown in Figure 4A).

$$^3J_{C4,H6R} = 3.58 + 0.11\cos(\omega) + 3.50\cos(2\omega) + 0.35\sin(\omega) - 0.57\sin(2\omega) \quad (\text{rms} = 0.38\ \text{Hz}) \quad (2)$$

$$^3J_{C4,H6S} = 3.60 + 0.50\cos(\omega) + 0.06\cos(2\omega) - 0.13\sin(\omega) - 3.46\sin(2\omega) \quad (\text{rms} = 0.44\ \text{Hz}) \quad (3)$$

Inclusion of the full hypersurface data (144 data points) and/or inclusion of additional terms to describe the dependence of $^3J_{C4,H6R/S}$ on $\theta$ yielded virtually identical equations. $^3J_{C4,H6R/S}$ calculated using eqs 2 and 3 were not predicted accurately using the previous Karplus equations;[31,32] rms deviations of 1.4 Hz were found between DFT-calculated couplings and those predicted by the previous treatments.

The effect of anti electronegative substituents on $^3J_{CCCH}$ is also observed in $^3J_{C6,H4}$ computed in **5**−**7** (Tables S1 and S2, Figure 4D). For **5**, $^3J_{C6,H4(eq)}$ is ~2.5 Hz smaller than $^3J_{C6,H4(ax)}$ (H4eq is anti to O5, whereas H4ax is gauche to O5), a decrease similar to that observed for $^3J_{C4,H6R/S}$. In addition to the "anti" effect, a small 1,3-effect appears to be present for $^3J_{C6,H4}$ in **5** in the *gg* rotamer (on $H4_{ax}$) and the *tg* rotamer (on $H4_{eq}$). This 1,3-effect decreases the observed $^3J_{C6,H4}$ by ~0.7 Hz. Similar effects were observed on $^3J_{C6,H4}$ in **6** and **7**, as shown in Figure 4D (Table S1). The introduction of an axial or equatorial O4 does not appear to influence $^3J_{C6,H4}$ significantly (i.e., couplings computed in **6** and **7** are similar to those computed in **5**), presumably because O4 cannot lie in the coupling plane in either orientation (i.e., a planar zigzag C6−C5−C4−O4 arrangement cannot be achieved). $^3J_{C6,H4}$ in **5**−**7** is also affected by $\theta$ (Figure 4D), exhibiting a range of ~1 Hz similar to that observed for $^3J_{C4,H6R/S}$.

**3. Three- and Two-Bond $^1$H−$^1$H Spin−Spin Coupling Constants.** $^3J_{H5,H6R}$ and $^3J_{H5,H6S}$ were computed previously in **5** using the limited set of staggered and eclipsed geometries given in Table 1.[6] Hypersurfaces were generated in the present work to more fully evaluate the effect of $\theta$ (Figure 5A, Figure

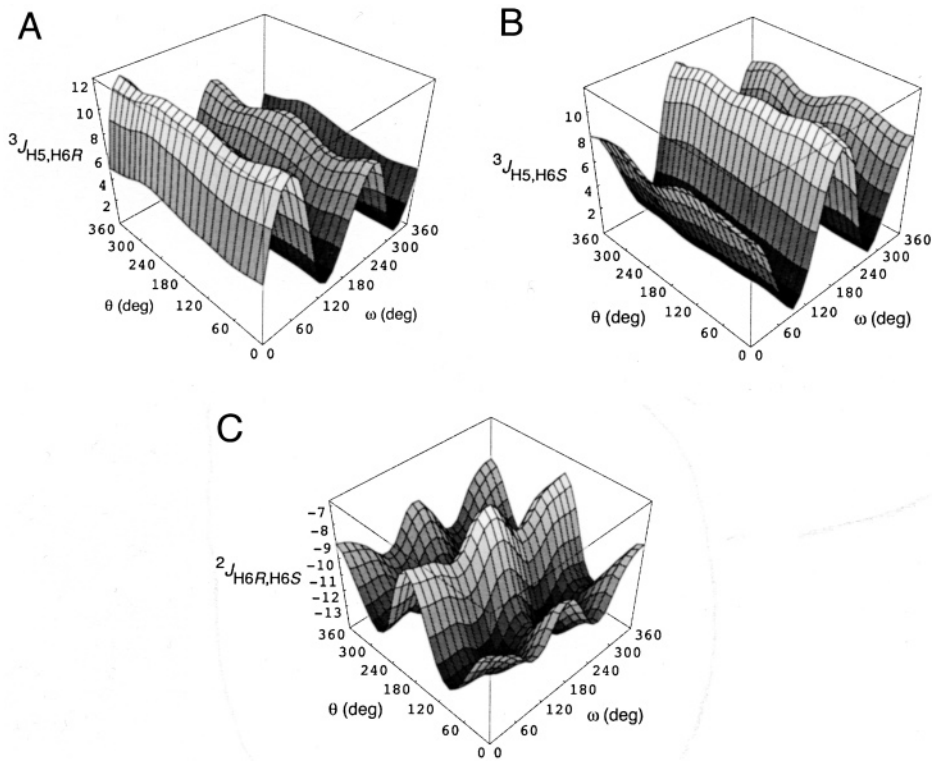


***Figure 6.*** (A) Hypersurface ($\omega/\theta$) calculated for $^3J_{H5,H6R}$ in **5**. (B) Hypersurface ($\omega/\theta$) calculated for $^3J_{H5,H6S}$ in **5**. (C) Hypersurface ($\omega/\theta$) calculated for $^2J_{H6R,H6S}$ in **5**.

6A and B). $^3J_{H5,H6R}$ and $^3J_{H5,H6S}$ exhibit approximately the same sensitivity to $\theta$ as do $^3J_{C4,H6R}$ and $^3J_{C4,H6S}$. In addition, the curves for $^3J_{H5,H6R}$ and $^3J_{H5,H6S}$ are phase-shifted by ~50°; similar behavior was observed for $^3J_{C4,H6R}$ and $^3J_{C4,H6S}$ (Figure 4). Importantly, corresponding curves calculated using a well-established empirically derived Karplus equation[33] are essentially superimposable on the DFT-computed curves (Figure 5A), thereby confirming the reliability of the DFT data.

In previous work, the dependencies of $^3J_{H5,H6R}$ and $^3J_{H5,H6S}$ on $\omega$ were described using DFT data obtained on nine completely optimized staggered and nine partially optimized eclipsed $\omega$ rotamers,[6] yielding eqs 4 and 5.

$$^3J_{H5,H6R} = 5.08 + 0.47\cos(\omega) - 0.12\cos(2\omega) + 0.90\sin(\omega) + 4.86\sin(2\omega) \quad (4)$$

$$^3J_{H5,H6S} = 4.92 - 1.29\cos(\omega) + 4.58\cos(2\omega) + 0.05\sin(\omega) + 0.07\sin(2\omega) \quad (5)$$

The above equations were not affected (i.e., rms errors differ by <0.1 Hz) when the same nine staggered conformers and 144 additional couplings from hypersurface calculations were included in the parametrizations. Equations for $^3J_{H5,H6R/S}$ were also derived by including additional terms to account for the small effect of $\theta$ (Figure 5A, Figure 6A and B), but this refinement did not improve the quality of the parametrization significantly.

$^2J_{H6R,H6S}$ in **5** is affected by both $\omega$ and $\theta$, but the dependence on $\theta$ is considerably greater (Figure 5B, Figure 6C). The latter conclusion is supported by data in Figure 5C and D, where computed $^2J_{HH}$ are plotted as a function of $\omega$ and $\theta$, respectively. In Figure 5C, where data for only the three perfectly staggered $\theta$ rotamers are shown, $^2J_{HH}$ is observed to shift to *more positive* (less negative) values when $\theta = 180°$ (Scheme 5).[6] In contrast, Figure 5D shows that coupling data as a function of $\theta$ for the three perfectly staggered $\omega$ rotamers are nearly identical. The hypersurface for $^2J_{H6R,H6S}$ is shown in Figure 6C. A simple equation derived from a restricted dataset was proposed previously[6] that related $^2J_{H6R,H6S}$ to $\omega$ and $\theta$. The additional hypersurface dataset obtained in this work yielded an improved equation (eq 6) with substantially reduced rms error.

$$^2J_{H6R,H6S} = -11.23 + 0.13\cos(\omega) + 0.74\cos(2\omega) - 0.82\cos(\theta) + 2.02\cos(2\theta) \qquad (\text{rms} = 0.51\ \text{Hz}) \quad (6)$$

**4. Two-Bond $^{13}C-^{13}C$ Spin−Spin Coupling Constants.** $^2J_{CCC}$ and $^2J_{COC}$ in saccharides have been studied previously, leading to an empirical projection resultant (PR) method that correlates the observed coupling to a projection resultant whose value depends on relative orientation of oxygen substituents on the coupled carbons.[3] In the present study, $^2J_{C4,C6}$ was studied to determine its sensitivity to $\omega$ and $\theta$.

Projection resultants determined for $^2J_{C4,C6}$ for the *gt*, *gg* and *tg* rotamers in **5** are +2.0, +0.5, and +0.5, respectively, yielding predicted couplings of +2−3 Hz, ~ −1 Hz, and ~ −1 Hz, respectively. These results are in qualitative agreement with the DFT-calculated couplings as a function of $\omega$ and $\theta$ (Table S3, Figure 7). Like $^2J_{CCH}$, a plot of $^2J_{CCC}$ vs $\omega$ contains a single maximum and a single minimum, and couplings of positive or negative sign. The dynamic range of ~4.5 Hz is smaller than that observed for $^2J_{CCH}$.

Introduction of O4 generally shifts $^2J_{C4,C6}$ to more negative values (Table S1), a result consistent with PR predictions;

(33) Donders, L. A.; de Leeuw, F. A. A. M.; Altona, C. *Magn. Reson. Chem.* **1989**, *27*, 556−563.

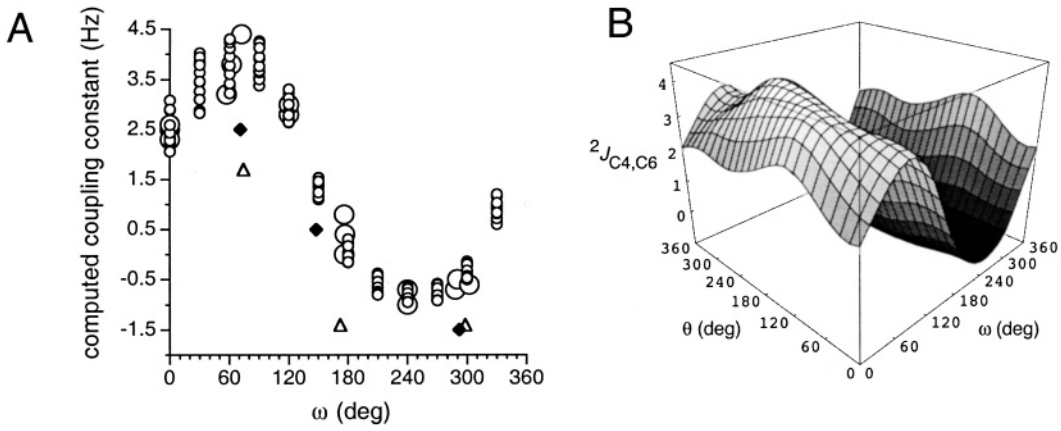


***Figure 7.*** (A) Dependence of $^2J_{C4,C6}$ in **5** on $\omega$. The vertical spread of points at discrete $\omega$ torsions (smaller open circles) indicates the effect of $\theta$. Larger open circles are data taken from Table S3 for staggered and eclipsed conformations about $\omega$. Data in triangles and diamonds were obtained from **6** and **7**, respectively (Table S1). (B) Hypersurface ($\omega/\theta$) calculated for $^2J_{C4,C6}$ in **5**.

projection resultants are shifted to more negative values by 0.5 unit, leading to the prediction of more negative couplings by ~1.5 Hz. The orientation of O4 appears to affect the magnitude of the negative shift for the *gt* and *tg* rotamers.

$^2J_{C4,C6}$ data calculated for **5** were fit to yield eq 7a, which reflects its dependence on $\omega$.

$$^2J_{C4,C6} = 1.36 + 1.03\cos(\omega) + 2.26\sin(\omega) \quad (\text{rms} = 0.3\ \text{Hz}) \quad (7a)$$

This equation was modified to account for the influence of O4 using data obtained on **6** and **7**, giving eq 7b.

$$^2J_{C4,C6} = 0.20 + 0.16\cos(\omega) + 1.34\sin(\omega) \quad (\text{rms} = 1.5\ \text{Hz}) \quad (7b)$$

The rms error for eq 7b is much larger than that for eq 7a due to the limited data presently available to define the O4 effect.

**5. One-Bond $^{13}$C−$^{13}$C Spin−Spin Coupling Constants and Bond-Length Considerations.** Previous work has shown[34] that $^1J_{CC}$ values in vicinal diol fragments (HO−C−C−OH) depend on the C−C and C−O torsion angles. Coupling is minimal and maximal for O−C−C−O torsion angles of ~0° and ~180°, respectively. Superimposed on this dependence are effects due to the C−O torsions; coupling is minimal and maximal when the H−O−C−C torsion angle is ~60° and ~180°, respectively.

The above relationships derived for a simple diol were tested in the $CH_2OH$ fragment where the C5−C6 and C6−O6 torsions are expected to modulate $^1J_{C5,C6}$. Data in Table S3 show that, within each C5−C6 rotamer (three staggered and three eclipsed), $^1J_{C5,C6}$ is larger when $\theta$ is ~180° (e.g., for *gt*, $^1J_{C5,C6}$ = 43.5, 42.0, and 48.0 Hz for $\theta$ = 57°, −48°, and 192°, respectively). The presence of one O6 lone pair anti to the C5−C6 bond reduces $^1J_{C5,C6}$ by ~5 Hz (Figure 8A). Data obtained from the full hypersurface are shown in Figure 8B (in which rotamers containing perfectly staggered $\theta$ are highlighted) and Figure 8C.

$^1J_{C5,C6}$ also depends on $\omega$, with smaller couplings observed for $\omega \approx 0°$ than for $\omega \approx 180°$. Based on data in Table S3, $^1J_{C5,C6}$ differs by ~5 Hz in these limiting conformations (Figure 8). These trends are similar to those reported in ethylene glycol.[34] Note that this behavior is different from that found for $^1J_{C4,C5}$, which shows essentially no dependence on $\omega$, as expected (Figure 8A). A brief discussion of the effect of $\omega$ on C5−C6, C6−H6*R*/*S*, C5−O5, and C6−O6 bond lengths and $^1J_{C5,C6}$ in **5** is found in the Supporting Information (Figures S1 and S2).

The $^1J_{C5,C6}$ data in Table S3 and the hypersurface results (Figures 8B and C) yielded eq 8, which correlates this coupling to $\omega$ and $\theta$.

$$^1J_{C5,C6} = 44.81 - 2.13\cos(\omega) - 0.59\cos(2\omega) - 3.57\cos(\theta) - 0.43\cos(2\theta) \quad (\text{rms} = 0.60\ \text{Hz}) \quad (8)$$

**6. Three-Bond $^{13}$C−$^{13}$C Spin−Spin Coupling Constants.** $^3J_{C1,C6}$ and $^3J_{C3,C6}$ values depend largely on the C1−O5−C5−C6 and C3−C4−C5−C6 torsion angles (Karplus curves), respectively, but a second-order dependence on the O5−C5−C6−O6 and C4−C5−C6−O6 torsion angles, respectively, is expected.[1,2] The latter dependencies arise from the effect of "in-plane" electronegative substituents, in the present case provided by O6 for specific values of $\omega$. Calculated couplings in **5** (153 datapoints) show a systematic change in both $^3J_{C1,C6}$ and $^3J_{C3,C6}$ as a function of $\omega$ (Figure S3); in these calculations the torsion angle between the coupled nuclei is essentially unchanged (~180°) due to constraints imposed by the pyranosyl ring. $^3J_{C1,C6}$ is maximal when $\omega$ = ~180° (*tg* rotamer), and $^3J_{C3,C6}$ is maximal when $\omega$ = ~+60 (*gt* rotamer); the two curves are complementary. Both couplings exhibit a small dependence on $\theta$. However, since **5** lacks OH substituents at C1, C3, and C4, trends observed in Figure S3 cannot be used quantitatively to assess $\omega$ in **1**−**4**. The potential for this application remains to be explored.

**7. Experimental Validation of Computed Couplings and Proposed Equations.** $^1$H and $^{13}$C NMR spectra of 4,6-*O*-ethylidene-α- and β-D-[4-$^{13}$C]-, [5-$^{13}$C]-, and [6-$^{13}$C]glucopyranoses (**8**α,β) and 4,6-*O*-ethylidene-α- and β-D-[6-$^{13}$C]-galactopyranoses (**9**α,β) contain experimental couplings that can be correlated with defined hydroxymethyl conformations (*tg* in *gluco*, *gg* in *galacto*). These couplings were compared to those predicted by the above equations and to those calculated in geometrically optimized conformers of 4,6-*O*-ethylidene-α-D-glucopyranose and 4,6-*O*-ethylidene-α-D-galactopyranose. These data (Table 2) show that corresponding experimental and calculated *J*-values differ by <1 Hz, suggesting that the

(34) Carmichael, I.; Chipman, D. M.; Podlasek, C. A.; Serianni, A. S. *J. Am. Chem. Soc.* **1993**, *115*, 10863−10870.

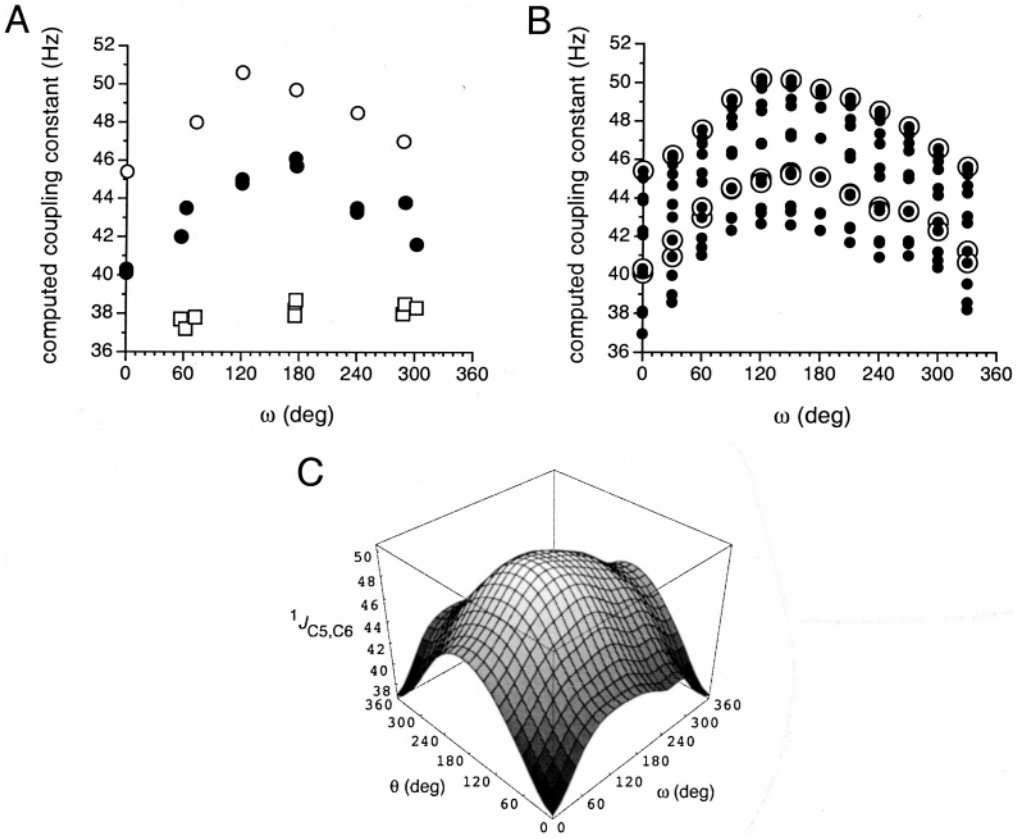


***Figure 8.*** (A) Dependencies of $^1J_{C5,C6}$ and $^1J_{C4,C5}$ in **5** on $\omega$ (data taken from Table S3). Filled circles, $^1J_{C5,C6}$ when $\theta = 60°$ and $-60°$; open circles, $^1J_{C5,C6}$ when $\theta = 180°$; open squares, $^1J_{C4,C5}$ (staggered $\omega$ rotamers only). (B) Similar plot as in part A but using data obtained from the full hypersurface. The vertical spread of points at discrete $\omega$ torsions (filled circles) indicates the effect of $\theta$. Open circles identify perfectly staggered $\theta$ rotamers. (C) Hypersurface ($\omega/\theta$) calculated for $^1J_{C5,C6}$ in **5**.

equations can be applied quantitatively in analyses of $CH_2OH$ conformation in **1**−**4**. Several trends emerged from the analysis of *J*-couplings in **8** and **9**.

In **8**, $^2J_{H6R,H6S}$ is −10.4 Hz for both anomers, in excellent agreement with the computed value of −10.4 Hz in **8**α (Table 2). The computed H−C−H bond angle in **8**α is 108.5°. The corresponding bond angle computed in **5** is 107.7° ± 0.4°.

Observed $^1J_{C6,H6R/S}$ in **8** depend significantly on C−H bond orientation, with the equatorial C6−H6*R* bond yielding a coupling ∼9 Hz larger than the axial C6−H6*S* bond. This difference suggests that the C6−H6*R* bond length is shorter than the C6−H6*S* bond length, a prediction consistent with expectations based on prior studies. Indeed, DFT calculations conducted on **8**α revealed $r_{C6,H6R}$ (eq) = 1.0932 Å and $r_{C6,H6S}$ (ax) = 1.1025 Å (in **9**α; $r_{C6,H6R}$ (ax) = 1.1037 Å and $r_{C6,H6S}$ (eq) = 1.0928 Å). In addition, $^1J_{C5,H5}$ is slightly larger in **8**α than in **8**$\beta$, again consistent with observations in D-glucopyranoses; this effect is attributed to the shorter C5−H5 bond in the α-pyranose caused by 1,4-interactions with lone pairs on the axial O1.[27]

$^1J_{C5,C6}$ is smaller in **9** than in **8** by ∼3 Hz. This difference is attributed to the change in the O5−C5−C6−O6 torsion angle from ∼180° in the latter to ∼60° in the former, which is expected to reduce the coupling (see $^1J_{CC}$ discussion below).[34]

$^3J_{C1,C6}$ and $^3J_{C3,C6}$ are consistently smaller in corresponding anomers of **9** than in **8**. For $^3J_{C1,C6}$, the difference is attributed to the presence of the "in-plane " O6 in *gluco* isomers, which enhances the coupling by ∼0.6 Hz.[1] For $^3J_{C3,C6}$, the effect is attributed mainly to the different configuration at C4, with an axial O4 reducing the coupling.[35a] Within anomeric pairs, the $\beta$-pyranose exhibits the larger $^3J_{C1,C6}$, as expected based on the orientational effects of O1.[35a,b]

**8. Average Computed *J*-Couplings in Staggered Hydroxymethyl Rotamers.** Average $J_{HH}$, $J_{CH}$, and $J_{CC}$ computed from hypersurface data by averaging the three staggered $\theta$ rotamers ($\theta = -60°$, 60°, and 180°) at each staggered value of $\omega$ are given in Table 3. $^2J_{CCH}$ sign predictions are also reported based on the projection rule;[23a] these predictions are in good agreement with the computed data, but the calculated coupling magnitudes are shifted to more negative values. This result is consistent with recent observations[24,25] and probably arises from limitations of the projection rule for predicting $^2J_{CH}$ not involving anomeric carbons or protons. The data in Table 3 provide an *average* dynamic range for each coupling, which is smaller than the actual dynamic range due to the averaging of $\theta$ effects.

**C. Experimental *J*-Couplings in 1−4 and Conformational Analysis. 1. Qualitative Treatment and Comparison to Theory.** Characteristic features of the $^1H$ and $^{13}C\{^1H\}$ NMR spectra of $^{13}C$-labeled methyl pyranosides are shown in Figures S4 and S5. The $^1H$ spectrum of methyl $\beta$-D-[4-$^{13}C$]galactopyranoside **4** (Figure S4) showed nonfirst-order behavior; the good agreement between the experimental and simulated spectra allowed extraction of accurate $J_{HH}$ and $J_{CH}$ values. The $^{13}C$-

(35) (a) Wu, J.; Bondo, P. B.; Vuorinen, T.; Serianni, A. S. *J. Am. Chem. Soc.* **1992**, *114*, 3499−3505. (b) King-Morris, M. J.; Serianni, A. S. *J. Am. Chem. Soc.* **1987**, *109*, 3501−3508.

***Table 2.*** Experimental *J*-Couplings[a] in $^{13}$C-Labeled 4,6-*O*-Ethylidene-α- and β-D-Gluco- (**8**) and Galactopyranoses (**9**) and Comparison with Calculated Couplings

| coupling | $J_{ex}$ (α)[b] | $J_{ex}$ (β)[b] | $J_{eq}$[c] | $J_{calc}$ (α)[d] |
|---|---|---|---|---|
| $^2J_{H6R,H6S}$ | −10.4 | −10.4 | −12.0/−11.8 | −10.4/−12.1 |
| $^3J_{H5,H6eq}$ | 4.9 | ∼4.6 | 4.5/4.9 | 4.9(−55.7°)/1.7 (−71°) |
| $^3J_{H5,H6ax}$ | | | 10.8/10.8 | 11.1(−176.2°)/1.7 (48.2°) |
| $^3J_{C4,H6eq}$ | 5.9 | 6.3 | 7.0/6.9 | 6.0 (−173.6°)/5.1 (169°) |
| $^3J_{C4,H6ax}$ | | | 3.2/2.8 | 3.3 (65.9°)/0.9 (−71.8°) |
| $^2J_{C5,H6eq}$ | −4.1 | −4.4 | −3.0/−3.0 | −3.6 (111.8°)/−4.8 (110.5°) |
| $^2J_{C5,H6ax}$ | | | −2.1/−2.3 | −3.0(109.7°)/6.3 (108.7°) |
| $^1J_{C6,H6eq}$ | 151.6 | 152.1 | | 153.0/154.5 |
| $^1J_{C6,H6ax}$ | 143.1 | 142.9 | | 141.7/137.5 |
| $^2J_{C6,H5}$ | −3.3 | | −2.8/−2.6 | −2.7 (108.9°)/2.4 (109.8°) |
| $^1J_{C5,C6}$ | 43.2 [40.3][e] | 43.1 [40.4] | 44.8/44.5 | 44.8/42.8 |
| $^2J_{C4,C6}$ | −1.6 [−2.2] | −1.5 [−2.1] | 0.04/−0.02 | −1.1 (108.4°)/−1.7 (109°) |
| $^3J_{C6,C1}$ | 3.8 [3.3] | 4.9 [4.3] | | 4.7/4.1 |
| $^3J_{C6,C3}$ | 3.2 [2.7] | 3.5 [3.1] | | 3.2/2.7 |
| $^3J_{C4,H2}$ | 1.0 | | | |
| $^2J_{C4,H3}$ | (−)[f]4.6 | | | |
| $^1J_{C4,H4}$ | 143.6 | 144.7 | | |
| $^2J_{C4,H5}$ | (−)1.6 | (−)2.2 | | |
| $^3J_{C4,CH}$ | ∼1.4 | ∼1.4 | | |
| $^3J_{C5,H1}$ | 6.4 | 0.9 | | |
| $^3J_{C5,H3}$ | 1.3 | | | |
| $^2J_{C5,H4}$ | (−)2.8 | (−)3.5 | | |
| $^1J_{C5,H5}$ | 148.8 | 146.2 | | |
| $^{4+4}J_{C5,CH}$ | 0.9 | | | |
| $^3J_{C6,H4}$ | ∼3.2 | ∼2.6 | | |
| $^3J_{C6,CH}$ | ∼1.2 | ∼1.2 | | |
| $^{3+3}J_{C4,C1}$ | 0 | 0 | | |
| $^2J_{C4,C2}$ | (+)3.7 | (+)3.4 | | |
| $^1J_{C4,C3}$ | 40.4 | 41.1 | | |
| $^1J_{C4,C5}$ | 37.5 | 38.1 | | |
| $^3J_{C4,CH}$ | br | br | | |
| $^3J_{C4,CH3}$ | 3.1 | 3.1 | | |
| $^2J_{C5,C1}$ | (−)1.8 | 0 | | |
| $^{3+3}J_{C5,C2}$ | 0 | 0 | | |
| $^{3+3}J_{C5,CH}$ | 2.4 | 2.5 | | |
| $^2J_{C6,CH}$[g] | 2.1 [1.9] | 2.1 [1.8] | | |
| $^3J_{C6,CH3}$ | 3.2 [2.9] | 3.2 [2.9] | | |

[a] In Hz. [b] Experimental couplings in aqueous solution at 298 K obtained from first-order analysis. [c] *J*-couplings predicted by equations that account for the effect of either ω alone or of ω and θ (see text). Two values are listed. Left entry: ω = 180° and θ = 60°. Right entry: ω = 182.7° and θ = 56.6° (torsions observed in the DFT-optimized structure of 4,6-*O*-ethylidene-α-D-glucopyranose **8**α). The following Karplus equations were used: eq 4 for $^3J_{H5,H6eq}$, eq 5 for $^3J_{H5,H6ax}$, eq 2 for $^3J_{C4,H6eq}$, eq 3 for $^3J_{C4,H6ax}$, eq 1a for $^2J_{C5,H6eq}$, eq 1b for $^2J_{C5,H6ax}$, eq 1c for $^2J_{C6,H5}$, eq 7b for $^2J_{C4,C6}$; eq 6 for $^2J_{H6R,H6S}$ and eq 8 for $^1J_{C5,C6}$. [d] DFT-calculated *J*-values in DFT-optimized 4,6-*O*-ethylidene-α-D-glucopyranose **8**α (first entry) and 4,6-*O*-ethylidene-α-D-galactopyranose **9**α (second entry). Relevant bond and torsion angles are given in parentheses. [e] Couplings in brackets are those observed in 4,6-*O*-ethylidene-α- and β-D-[6-$^{13}$C]galactopyranoses. [f] Signs shown in parentheses were predicted by the projection rule ($^2J_{CH}$, ref 23a) and the projection resultant method ($^2J_{CC}$, ref 3). [g] Signs for these couplings are unknown.

***Table 3.*** Averaged Calculated *J*-Couplings in Hydroxymethyl Group Fragments for Staggered Rotamers about ω and θ[a]

| coupling | *gg* (ω = −60°) | *gt* (ω = 60°) | *tg* (ω = 180°) |
|---|---|---|---|
| $^2J_{H6R,H6S}$ | −10.8 | −10.9 | −10.0 |
| $^2J_{C5,H6R}$ | +3.4 (+)[b] | −4.7 (−) | −3.0 (−) |
| $^2J_{C5,H6S}$ | −3.8 (−) | +3.4 (+) | −4.0 (−) |
| $^2J_{C6,H5}$ | +2.6 (+) | −4.0 (−) | −3.0 (−) |
| $^2J_{C4,C6}$ | −0.2 | +3.8 | 0.1 |
| $^3J_{H5,H6R}$ | 0.9 | 10.8 | 4.7 |
| $^3J_{H5,H6S}$ | 2.8 | 2.2 | 11.1 |
| $^3J_{C4,H6R}$ | 1.7 | 1.4 | 6.7 |
| $^3J_{C4,H6S}$ | 6.7 | 0.8 | 3.4 |

[a] Couplings were computed from hypersurface data by averaging the three staggered θ rotamers (θ = −60°, 60°, and 180°) at each staggered value of ω. Since some couplings exhibit a specific dependence on θ (see text), use of these average couplings to fit experimental data is valid only when perfectly staggered ω rotamers, and equal populations of perfectly staggered θ rotamers, are present in solution. [b] Values in parentheses are signs predicted by the projection rule.[23a]

{$^1$H} spectrum of methyl α-D-[6-$^{13}$C]galactopyranoside **3** (Figure S5) shows long-range coupling to both C1 and C3, one-bond coupling to C5, and no coupling to C2, C4, and the aglycone CH3.

Experimental $J_{HH}$ values in **1**−**4** (Table 4) agree well with those reported previously[14] except for $^3J_{H5,H6R}$ and $^3J_{H5,H6S}$ in **3**. The latter couplings were confirmed via spectral simulation (Figure S4) and are in agreement with those reported by Tvaroska et al..[32] Stereochemical assignments of the H6*R* and H6*S* signals in **1**−**4** were made according to Ohrui et al.[36] (i.e., H6*S* downfield of H6*R* in *gluco*, H6*R* downfield of H6*S* in *galacto*).

Experimental $J_{CH}$ values in **1**−**4** are given in Table 5. $^1J_{C4,H4}$ is larger in **3**/**4** than in **1**/**2**. This enhancement may be attributed to C−H bond orientation (axial vs equatorial) and/or C4−O4 bond conformation. The equatorial C4−H4 bond in **3**/**4** is expected to be shorter than the axial C4−H4 bond in **1**/**2**, possibly leading to larger $^1J_{CH}$ in the former. However, an axial

(36) (a) Ohrui, H.; Nishida, Y.; Higuchi, H.; Hori, H.; Meguro, H. *Can. J. Chem.* **1987**, *65*, 1145−1153. (b) Ohrui, H.; Nishida, Y.; Meguro, H. *Agric. Biol. Chem.* **1984**, *48*, 1049−1053. (c) Hori, H.; Nakajima, Y.; Nishida, H.; Ohrui, H.; Meguro, H. *J. Carbohydr. Chem.* **1986**, *5*, 585−600.

***Table 4.*** Experimental $^1H-^1H$ Spin−Spin Coupling Constants[a] in **1**−**4**

| coupling | α-D-Glc **1** | β-D-Glc **2** | α-D-Gal **3** | β-D-Gal **4** |
|---|---|---|---|---|
| $^3J_{H1,H2}$ | 3.8 (3.8)[b] | 8.0 (8.0) | 3.9 (4.0) | 8.0 (7.9) |
| $^3J_{H2,H3}$ | 9.8 (9.8) | 9.5 (9.4) | 10.3 (10.3) | 9.9 (9.9) |
| $^3J_{H3,H4}$ | 9.2 (9.1) | 9.2 (9.2) | 3.4 (3.4) | 3.5 (3.4) |
| $^3J_{H4,H5}$ | 10.0 (10.1) | 10.0 (9.7) | 1.2 (1.0) | 1.1 (1.1) |
| $^3J_{H5,H6R}$ | 5.6 (5.5) [5.4][c] | 6.2 (6.0) [5.9] | 8.2 (7.2) [8.3] | 7.9 (7.9) [7.6] |
| $^3J_{H5,H6S}$ | 2.3 (2.3) [2.2] | 2.3 (2.3) [2.0] | 4.2 (5.2) [4.0] | 4.4 (4.4) [4.4] |
| $^2J_{H6R,H6S}$ | −12.3 (−12.3) | −12.4 (−12.3) | −11.7 (−11.7) | −11.8 (−11.7) |

[a] In Hz ±0.1 Hz, $^2H_2O$ solvent, 30 °C. [b] Data in parentheses were taken from Podlasek et al..[14] [c] Data in brackets were taken from Tvaroska et al..[32]

***Table 5.*** Experimental $^{13}C-^1H$ Spin−Spin Coupling Constants[a] in **1**−**4**

| coupling | α-D-Glc **1** | β-D-Glc **2** | α-D-Gal **3** | β-D-Gal **4** |
|---|---|---|---|---|
| $^1J_{C4,H4}$ | 144.4 | 144.8 | 146.4 | 146.3 |
| $^1J_{C5,H5}$ | 144.3 | 141.8 | 143.4 | 140.7 |
| $^1J_{C6,H6R}$ | 143.3 | 143.2 | 145.2 | 145.5 |
| $^1J_{C6,H6S}$ | 144.2 | 144.4 | 142.5 | 142.9 |
| $^2J_{C4,H3}$ | −4.7 | −4.8 | +1.7 | +1.6 |
| $^2J_{C4,H5}$ | −2.9 | −2.9 | +3.1 | +3.3 |
| $^2J_{C5,H4}$ | −3.9 | −4.0 | ±1.1 | ±1.0 |
| $^2J_{C5,H6R}$ | −1.9 | −2.5 | −5.0 | −5.0 |
| $^2J_{C5,H6S}$ | −1.4 | −1.1 | ±0.8[e] | ±0.2[e] |
| $^2J_{C6,H5}$ | −1.4 | −2.2 | −5.2 | −5.5 |
| $^3J_{C4,H2}$ | 1.0 | 1.1 | 0.8 | 0.6 |
| $^3J_{C4,H6R}$ | 1.1 (1.1)[d] | 1.2 (1.0) | 1.9 (0.9) | 1.9 (1.5) |
| $^3J_{C4,H6S}$ | 2.8 (2.9) | 2.4 (2.4) | 1.7 (3.7) | 1.8 (4.0) |
| $^3J_{C5,H1}$ | obsc[b] | 1.1 | 6.3 | 0.9 |
| $^3J_{C5,H3}$ | 0.9 | 1.1 | 0.4 | nc[c] |
| $^3J_{C6,H4}$ | 3.6 | 3.6 | 1.0 | 1.0 |

[a] In Hz ±0.1 Hz, $^2H_2O$ solvent, 30 °C. Signs determined via the projection rule[23a] and/or spin simulation. [b] obsc = signal obscured by the HOD signal. [c] nc = no coupling observed, $|J| \leq 0.5$ Hz. [d] Values in parentheses were reported by Tvaroska et al..[32] [e] Signs were taken as (+) in calculations of $\omega/\theta$ rotamer populations (see text).

O4 may disrupt directional intramolecular H-bonding between the adjacent equatorial OH groups of **1**/**2**, resulting in an increased population (relative to **1**/**2**) of the C4−O4 rotamer having OH4 anti to H4 in **3**/**4**. In the latter rotamer, no O4 lone pairs are anti to the C4−H4 bond, and no C4−H4 bond elongation occurs.

$^1J_{C5,H5}$ exhibits a dependence on anomeric configuration, with α-anomers yielding slightly larger couplings than β-anomers. This result is consistent with prior studies of oxygen lone pair effects on saccharide C−H bond lengths.[27] The axial C1−O1 bond in α-anomers provides O1 lone pairs in a 1,4-orientation to the C5−H5 bond. The resulting bond shortening, which is absent in β-anomers, presumably enhances $^1J_{C5,H5}$. A similar argument was made recently in studies of $^2H$ nuclear quadrupolar coupling constants in aldopyranosyl rings.[37]

$^2J_{C4,H3}$, $^2J_{C4,H5}$, and $^2J_{C5,H4}$ have negative signs in **1**/**2** and positive signs (when detected) in **3**/**4**. These results are consistent with sign predictions based on the projection rule;[23a] for **1**/**2** and **3**/**4**, projections of 0 and +1.5 are obtained, respectively, for each of these couplings, leading to predicted (−) and (+) signs, respectively. However, despite similar projections, $^2J_{C4,H3}$, $^2J_{C4,H5}$, and $^2J_{C5,H4}$ vary considerably, indicating that a general empirical method to predict coupling magnitudes is error-prone due to differences in coupling pathway structure and C−O bond conformations.

(37) Bose-Basu, B.; Zajicek, J.; Bondo, G.; Zhao, S.; Kubsch, M.; Carmichael, I.; Serianni, A. S. *J. Magn. Res.* **2000**, *144*, 207−216.

***Table 6.*** Experimental $^{13}C-^{13}C$ Spin−Spin Coupling Constants[a] in **1**−**4**

| coupling | α-D-Glc **1** | β-D-Glc **2** | α-D-Gal **3** | β-D-Gal **4** |
|---|---|---|---|---|
| $^1J_{C3,C4}$ | 38.5 | 39.3 | obsc[b] | 38.6 |
| $^1J_{C4,C5}$ | 40.4 | 41.0 | 38.2 | 38.5 |
| $^1J_{C5,C6}$ | 43.3 | 43.3 | 44.7 | 44.8 |
| $^2J_{C1,C5}$ | −2.0[d] | nc[c] | −2.0[d] | nc |
| $^2J_{C2,C4}$ | +3.1[e] | +2.7[e] | nc | nc |
| $^2J_{C3,C5}$ | +1.8[e] | obsc | *nc* | +1.6[e] |
| $^2J_{C4,C6}$ | nc | *nc* | nc | nc |
| $^3J_{C1,C6}$ | 3.3 | 4.2 | 3.5 | 4.4 |
| $^3J_{C2,C5}$ | obsc | nc | 1.3 | nc |
| $^3J_{C3,C6}$ | 3.7 | ∼4.3 | 3.8 | 4.2 |

[a] In Hz ±0.1 Hz, $^2H_2O$ solvent, 30 °C. [b] obsc = signal obscured. [c] nc = no coupling observed, $|J| \leq 0.5$ Hz. [d] Sign based on $^{13}C-^{13}C$ COSY-45 data.[44] [e] Sign predicted by the projection resultant method.[3]

Experimental $^2J_{C5,H6R}$ and $^2J_{C5,H6S}$ range from −1.9 Hz to −5.0 Hz and ±0.2 Hz to −1.4 Hz, respectively, whereas $^2J_{C6,H5}$ ranges from −1.5 Hz to −5.5 Hz. These couplings lie within the range predicted from the calculations (Figures 2 and 3). Large shifts to more negative couplings are observed for $^2J_{C5,H6R}$ and $^2J_{C6,H5}$ upon converting **1**/**2** to **3**/**4**. This shift is consistent qualitatively with a more populated *tg* rotamer in Gal, at the expense of the *gg* rotamer population. The *positive* contribution made to the experimental couplings by the *gg* rotamer is replaced by a *negative* contribution made by the *tg* rotamer. This shift in populations exerts a much smaller effect on $^2J_{C5,H6S}$, since both *gg* and *tg* rotamers are associated with negative couplings (Figures 2 and 3).

$^3J_{C4,H2}$ Values are slightly larger in **1**/**2** than in **3**/**4**, possibly due to a small in-plane effect from the equatorial O4.[14] $^3J_{C4,H6R}$ and $^3J_{C4,H6S}$ in **1**−**4** differ considerably from those reported recently.[32] The couplings in Table 5 were confirmed through spectral simulation. Previously reported couplings[32] were measured from selective excitation experiments, but the resonance frequencies for the H6 protons differ by ∼7 Hz in **3** and ∼23 Hz in **4** at 600 MHz, which precludes determinations of accurate $^3J_{CH}$ using first-order approaches. Presumably this complication is responsible for the observed differences.

$^3J_{C5,H1}$ in **1**−**4** shows the expected dependence on anomeric configuration, with larger couplings observed in α-anomers (C5 anti to H1).[35a] $^3J_{C6,H4}$ is considerably larger in **1**/**2** (∼3.5 Hz) than in **3**/**4** (∼1.1 Hz) despite the gauche arrangement between C6 and H4 in all compounds. The smaller coupling in **3**/**4** is consistent with our theoretical findings (Figure 4D).

Experimental $J_{CC}$ values in **1**−**4** are given in Table 6. $^1J_{C4,C5}$ is smaller in **3**/**4** compared to **1**/**2**, whereas the opposite is observed for $^1J_{C5,C6}$. The O4−C4−C5−O5 torsion angle changes from ∼180° in **1**/**2** to ∼60 in **3**/**4**, and $^1J_{CC}$ is expected to decrease;[34] the effect of the C4−O4 torsion on $^1J_{C4,C5}$, which can be substantial, is assumed to be negligible in this case.

Similar arguments explain the $^1J_{C5,C6}$ data; the slightly larger values in **3**/**4** reflect a greater contribution by the *tg* rotamer in which O5 and O6 are anti, thus increasing the coupling. Again, C6−O6 torsion effects are assumed to be minimal.

$^2J_{C1,C5}$ depends on anomeric configuration:[35b] ∼ −2 Hz for α-anomers and ∼0 Hz for *β*-anomers. $^2J_{C2,C4}$ is large and positive in **1**/**2** and ∼0 Hz in **3**/**4**, as expected based on the projection resultant method.[3] $^2J_{C4,C6}$ is ∼0 Hz in **1**−**4**; conformational averaging of the *gg* and *gt* forms for **1**/**2**, and the *gt* and *tg* forms for **3**/**4**, is expected to yield small $^2J_{C4,C6}$ (Figure 7).

$^3J_{C1,C6}$ and $^3J_{C3,C6}$ depend on the C1−O5−C5−C6 and C3−C4−C5−C6 torsion angles;[35a,b] in both cases, this torsion angle in **1**−**4** is ∼180°. Small deviations in the observed coupling are probably due to small changes in the torsion angle between anomers and/or to in-plane electronegativity effects; $^3J_{C1,C6}$ is enhanced in *β*-anomers relative to α-anomers due to an in-plane equatorial O1.[1,35b] In addition, the *tg* rotamer will enhance $^3J_{C1,C6}$ due to an in-plane O6; the small difference between **1** and **3**, and between **2** and **4**, may be due to the expected larger population of *tg* rotamer in Gal, which will enhance the observed coupling. For $^3J_{C3,C6}$, the *gt* rotamer is expected to enhance the coupling, due to an in-plane O6. Both Glc and Gal isomers show an enhancement in $^3J_{C3,C6}$ in the *β*-anomer; this result may reflect, at least partly, an increase in the *gt* rotamer in *β*-anomers (see below).

**2. Hydroxymethyl Rotamer (*ω*) Analysis in 1−4.** All regressions and multilinear fits were conducted using a Fortran 77 program, Chymesa, written in our laboratory (a copy of this program can be obtained by contacting the authors). This program allows for selection of the protocol to be used for the regression or fit, i.e., the set of experimental *J*s used in the calculation, the source of limiting *J* values for the *gt*, *gg*, and *tg* rotamers, and the weight attributed to each *J* in the fit. The latter weight is used in the determination of the overall root-mean-square (rms) error between the experimental and calculated *J*s. The use of weighting factors accounts for differences in the quality of the equations available for each coupling pathway. The program also allows the selection of ranges for each rotamer population in order to partially constrain the calculation if judged appropriate on the basis of additional experimental or theoretical data. However, in the present work, this feature was not applied. Instead, mole fractions of all conformers were allowed to vary from 0 to 1 during the fit. In addition, an equal weighting factor of 1 was applied to all *J*s used to calculate equilibrium populations.

Three analyses were performed on **1**−**4**, denoted as $A_x$, $B_x$, and $C_x$. The results of these calculations are shown in detail in Tables S4−S7 and are summarized in Table 7. In these calculations, the experimental *J*-couplings were analyzed in the conventional manner, namely, as probes of *ω*; the *θ* dependencies will be considered below. In $A_1$−$A_3$, *ω* populations were obtained using only $^3J_{H5,H6R/S}$. In $B_1$−$B_3$, *ω* populations were obtained using only $^3J_{C4,H6R/S}$. In $C_1$−$C_4$, multilinear fits were made using six experimental *J*s ($^3J_{H5,H6R/S}$, $^3J_{C4,H6R/S}$, $^2J_{C6,H5}$, $^2J_{C4,C6}$). Two results were obtained for the $C_1$−$C_3$ analyses: (1) the "best" fit (i.e., that which gave the lowest overall rms error between the experimental and calculated *J*s) and (2) a statistical analysis consisting of average values and standard deviations for the *gt*, *gg*, and *tg* populations derived from an ensemble of acceptable fits. The latter included calculations characterized by an overall rms error within 10% of the lowest rms error found among all analyses. This range corresponds to an ∼0.1 Hz uncertainty in the rms error, which is equal to the precision of the experimental *J*s.

***Table 7.*** Summary of *ω* and *θ* Rotamer Populations Determined by Single *ω* Analysis and Correlated *ω*/*θ* Analysis[a] in **1**−**4**

| | rotamer populations (%) | | | | | |
|---|---|---|---|---|---|---|
| compound | *gt* | *gg* | *tg* | *g+* | *g−* | trans |
| **1** | 53 (2) | 40 (2) | 7 (2) | | | |
| | 51 | 41 | 8 | 25 | 55 | 20 |
| **2** | 61 (2) | 31 (2) | 8 (2) | | | |
| | 59 | 32 | 9 | 21 | 59 | 20 |
| **3** | 74 (4) | 3 (2) | 23 (4) | | | |
| | 74 | 0 | 26 | 27 | 36 | 37 |
| **4** | 72 (4) | 3 (2) | 25 (4) | | | |
| | 71 | 0 | 29 | 23 | 39 | 38 |

[a] Single *ω* analysis (first entry); data obtained by the $C_3$ fitting method. Correlated *ω*/*θ* analysis (second entry); data obtained by the $A_3$ fitting method. See text and Tables S4−S11 in Supporting Information. Values in parentheses are the respective standard deviations in the population.

The subscripts in the $A_x$, $B_x$, and $C_x$ series of calculations designate how the limiting *J*-values were chosen. In $A_1$, $B_1$, and $C_1$, an equilibrium between the three *perfectly staggered* *ω* rotamers (*ω* = 60°, −60°, and 180°) was considered. Limiting *J*-values were calculated from the *average* of hypersurface data over the three perfectly staggered *θ* rotamers at a specific *ω*; these values are reported in Table 3. This approach assumes that only perfectly staggered *ω* rotamers are present in solution and that the populations of the three *θ* rotamers are equal.

For $A_2$, $B_2$, and $C_2$, DFT-calculated *J*-values for nine freely optimized (*ω*, *θ*) rotamers (Tables 1, S2 and S3 for $^2J_{C6,H5}$, $^3J_{C4,H6R/S}$, and $^2J_{C4,C6}$, and Table 2 in ref 6 for $^3J_{H5,H6R/S}$) were used to calculate limiting *J*s for the *ω* rotamer from the average over the three corresponding *θ* conformations. For example, $^3J_{C4,H6R}$ for *gt* is (1.2 + 1.7 + 0.6)/3 = 1.16 Hz. Like $A_1$, $B_1$, and $C_1$, no preference for a specific *θ* orientation is assumed.

For $A_3$, $B_3$, and $C_3$, calculations were conducted assuming a three-state equilibrium, but limiting *J*-values were calculated using parametrized equations. Average torsion angles for *gt*, *gg*, and *tg* in the *gluco* (65°, −66.5°, and 175°) and *galacto* (63.8°, −52° and 178.4°) configurations were taken from statistical studies of X-ray structures[38a] and assumed to be reasonable first-order approximations of the torsions in **1**−**4**.

Equations 4 and 5 were used to treat $^3J_{H5,H6R}$ and $^3J_{H5,H6S}$, and eqs 2 and 3 were used to treat $^3J_{C4,H6R/S}$ for the regression and multilinear fits. Limiting values of $^2J_{C6,H5}$ were derived from eq 1c, and limiting values of $^2J_{C4,C6}$ were estimated from eq 7b. Contributions by *θ* were assumed to be uniform.

The analyses (Table 7) show that *gt* and *gg* predominate, and *tg* is almost absent, in **1**/**2**. In contrast, the *gg* population is much reduced compared to *tg* and *gt* in **3**/**4**. These results are consistent with the strong influence of C4 configuration on the distribution of *ω* rotamers in saccharides.[38,39] However, we find that *gt* predominates over *gg* in **1**/**2**, contrary to prior reports.[39] Furthermore, for **3**/**4**, very little *gg* rotamer was found, whereas

(38) (a) Marchessault, R. H.; Perez, S. *Biopolymers* **1979**, *18*, 2369−2374. (b) Rockwell, G. D.; Grindley, T. B. *J. Am. Chem. Soc.* **1998**, *120*, 10953−10963. (c) Kuttel, M.; Brady, J. W.; Naidoo, K. J. *J. Comput. Chem.* **2002**, *23*, 1236−1243. (d) Behrends, R.; Cowman, M. K.; Eggers, F.; Eyring, E. M.; Kaatze, U.; Majewski, J.; Petrucci, S.; Richmann, K.-H.; Riech, M. *J. Am. Chem. Soc.* **1997**, *119*, 2182−2186.

*gg* populations as large as 20% were reported previously.[39] We attribute these differences to the use of multiple *J*-couplings in the determinations; if the analyses are restricted to $^3J_{HH}$ only, populations similar to those reported previously are obtained. In **1**/**2**, however, analyses based solely on $^3J_{HH}$ frequently lead to negative *tg* populations. In contrast, the multiple *J* analysis yields positive populations for all three rotamers, thereby lending greater confidence to the results.

For analyses based only on two *J* values (i.e., $A_x$ or $B_x$), significant negative *tg* rotamer populations in **1**/**2** are observed in only a few cases, suggesting that the selected limiting *J*s in the three $\omega$ rotamers are reasonable approximations (see Supporting Information). Importantly, for each compound, and for each of the $A_x$ and $B_x$ series, relatively small differences (less than ±5% from the average values) in rotamer populations are observed as the source of limiting *J*s was varied. Limiting values derived from the parametrized equations or from DFT data yielded nearly the same results. However, discrepancies (ca. ±10−15%) were observed between populations estimated solely from $^3J_{H5,H6R/S}$ or solely from $^3J_{C4,H6R/S}$.

These findings stimulated the $C_x$ series of analyses in which all available couplings were incorporated in the multilinear fit. For **1**−**4**, the C3 fits yielded the most accurate solutions to the equations. These analyses suggest that $\omega$ rotamers are not perfectly staggered in solution and that estimates of populations based on torsion angles observed in crystal structures are more accurate.

A comparison of $\omega$ populations determined by regression analysis or through multilinear fit for **1**/**2** reveals a small increase and decrease (∼10%), respectively, in the populations of *gt* and *gg* in the $\beta$-pyranose relative to the α-pyranose, suggesting an effect of anomeric configuration on $\omega$ populations (Table 7). This effect appears absent in **3**/**4**.

**3. Distribution of Nine ($\omega$,$\theta$) Rotamers in 1−4 Through Multilinear Fit.** In previous work,[6] rotamer populations having $\theta = 180°$ (trans) in mono-, di-, and trisaccharides were estimated from $^2J_{H6R,H6S}$, assuming perfectly staggered $\omega$ and $\theta$ rotamers and a similar distribution of $\theta$ rotamers in each of the three $\omega$ rotamers. Four limiting *J*-values were used, and no distinction was made between *gt* and *gg* and between *g*+ and *g*− rotamers. This analysis suggested that gauche C5−C6−O6−O6H rotamers are preferred in most saccharides and that as bulkier substituents at O6 are introduced, the population of trans rotamer increases. The percentage of trans rotamers for methyl $\beta$-D-gluco- and galactopyranosides was in agreement with that estimated from $^3J_{HCOH}$ (H6*R*/*S*−C6−O6−H pathway).[40]

The preceding discussion showed that $\omega$ rotamer populations can be determined using five *J*-values through multilinear regression. This approach was extended to evaluate both $\omega$ and $\theta$ using twelve *J*-values sensitive either to $\omega$ alone or to both $\omega$ and $\theta$. $^2J_{C5,H6R/S}$ are sensitive to $\omega$ and $\theta$ (Figures 2 and 3); $^2J_{C6,H5}$ also exhibits a dependence on $\theta$, albeit to a lesser extent. The effect of $\theta$ on $^3J_{H5,H6R/S}$ and $^3J_{C4,H6R/S}$ is small (∼1.0 Hz) and less easily parametrized. Present and previous[6] work has shown that $^2J_{H6R,H6S}$ is more sensitive to $\theta$ than to $\omega$. $^2J_{C4,C6}$ provided information about $\omega$ alone, while $^1J_{C5,C6}$ is influenced by $\omega$ and $\theta$. $^1J_{C6,H6R/S}$ values were used qualitatively to assess hydroxymethyl conformation.[6]

***Table 8.*** Summary of $\theta$ Rotamer Populations in Different $\omega$ Rotamers in **1**−**4**[a]

| | rotamer populations (%) | | | | | | | | |
|---|---|---|---|---|---|---|---|---|---|
| | $\omega = gt$ | | | $\omega = gg$ | | | $\omega = tg$ | | |
| compound | *g*+ | *g*− | trans | *g*+ | *g*− | trans | *g*+ | *g*− | trans |
| **1** | 15(9) | 27(7) | 9(5) | 7(5) | 25(6) | 9(6) | 3(3) | 3(3) | 2(2) |
| **2** | 14(8) | 32(7) | 13(5) | 4(3) | 23(5) | 5(4) | 3(3) | 4(3) | 2(2) |
| **3** | 19(9) | 21(9) | 34(4) | 0(0) | 0(0) | 0(0) | 8(7) | 15(7) | 3(3) |
| **4** | 15(9) | 21(9) | 35(4) | 0(1) | 0(1) | 0(1) | 8(7) | 18(7) | 3(3) |

[a] Data obtained by the $A_3$ fitting method; see text and Tables S8−S11 in Supporting Information. Values in parentheses are the respective rms errors in the population.

In the multilinear fitting procedure described below, different weights were applied to the couplings to account for (a) differences in the precision to which they are known from experiment, (b) the different quality of the equations (rms errors), and (c) possible contributions to their magnitudes from factors (e.g., lone pair effects on $^1J_{CH}$) which were neglected owing to a lack of sufficient data. The following weighting factors were chosen for the fits: 1.0 ($^3J_{H5,H6R/S}$, $^3J_{C4,H6R/S}$, $^2J_{C5,H6R/S}$, $^2J_{C6,H5}$, $^2J_{H6R,H6S}$, and $^1J_{C5,C6}$), 0.1 ($^2J_{C4,C6}$), and 0.01 ($^1J_{C6,H6R/S}$).

Nine $\omega/\theta$ conformers were considered: $\omega \approx 60°$, −60°, or 180°, in each case with $\theta \approx 60°$, −60°, or 180°. This model assumes that no intermediate states exist in solution with detectable lifetimes and that all states are independent. Rotamer populations were varied from 0 to 100% in 2% increments, and the best analyses were defined as those resulting in the smallest rms errors between the calculated and experimental couplings.

Three multilinear fits ($A_1$−$A_3$ in Tables S8−S11) were performed. In $A_1$, limiting *J*-values and $\omega$ and $\theta$ torsion angles were taken from DFT calculations of the nine completely optimized staggered conformers (Tables 1, S2, and S3). In $A_2$ and $A_3$, parametrized equations (eqs 4/5 for $^3J_{H5,H6R/S}$, eqs 2/3 for $^3J_{C4,H6R/S}$, eqs 1a/b for $^2J_{C5,H6R/S}$, eq 1c for $^2J_{C6,H5}$, eq 8 for $^1J_{C5,C6}$, eq 7b for $^2J_{C4,C6}$, eq 6 for $^2J_{H6R,H6S}$) and elsewhere (ref 6 for $^1J_{C6,H6R/S}$) were used to back-calculate limiting couplings, assuming either perfectly staggered $\omega$ and $\theta$ conformers ($A_2$) or the torsion angles used in $A_1$ ($A_3$).

The results of these analyses are given in Tables S8−S11. The set of populations of the nine $\omega/\theta$ conformers that produced the lowest weighted rms error is shown for $A_1$−$A_3$, followed by statistical data with average populations and standard deviations (5% tolerance from the lowest rms value), as discussed above for the regression analyses to assess $\omega$ alone. The sums of populations for $\omega = 60°$, −60°, or 180° rotamers over the corresponding three $\theta = 60°$, −60°, or 180° rotamers, and conversely, sums of populations for $\theta = 60°$, −60°, or 180° rotamers over the corresponding three $\omega = 60°$, −60°, or 180° rotamers, were calculated. Error analyses are provided in the form of the overall rms error of the "best" run and in the individual errors in each *J*, estimated from the difference between the predicted *J* and the corresponding experimental value. Both weighted [rms (1)] and unweighted [rms (2)] errors were determined. However, to determine the best fit among all calculations, weighted rather than unweighted rms errors were used for the reasons explained above. The results are summarized in Table 8.

(39) (a) Bock, K.; Duus, J. O. *J. Carbohydr. Chem.* **1994**, *13*, 513−543. (b) Nishida, Y.; Hori, H.; Ohrui, H.; Meguro, H. *J. Carbohydr. Chem.* **1988**, *7*, 239−250.
(40) Fraser, R. R.; Kaufman, M.; Morand, P.; Govil, G. *Can. J. Chem.* **1969**, *47*, 403−409.

**a. Distribution of ($\omega$,$\theta$) Rotamers in 1/2.** Data in Tables 7 and 8 confirm the validity of the nine-state equilibrium model. For **1**/**2**, the weighted rms errors of the best fits for the $A_1-A_3$ multilinear regressions were consistently <0.7 Hz, while the unweighted rms errors ranged from 0.8 to 1.2 Hz. All regressions predicted time-average couplings within 0.5−1.5 Hz of the experimental values except for $^1J_{C6,H6R/S}$. In all runs, $^1J_{C6,H6R}$ and $^1J_{C6,H6S}$ were not accurately predicted (errors up to ~3 Hz), which was expected since the equations were qualitative. Although the ranges of overall rms errors for $A_1-A_3$ were small for **1**/**2**, the $A_3$ regressions consistently produced the smallest rms errors. This finding suggests that $\omega$ and $\theta$ in solution deviate from those in perfectly staggered geometries.

The distribution of $\omega$ and $\theta$ rotamers predicted from the $A_1-A_3$ analyses are similar for **1** and **2** (Table 7). For **1**, the *gg* and *gt* rotamers are roughly equally populated and account for >~90% of the $\omega$ populations, with *tg* represented by <10%. In contrast, data for **2** suggest a preference of *gt* over *gg* (~2-fold), with *tg* still representing <10% of the population. Thus, a small effect of anomeric configuration on $\omega$ distribution is observed in the *gluco* anomers. An analysis of $\theta$ reveals a preference for *g*− in **1**/**2** (Table 7).

More revealing is the *distribution* of $\theta$ rotamers within specific $\omega$ rotamers (Table 8). The data suggest that $\omega$ and $\theta$ are not conformationally coupled, that is, the distribution of $\theta$ rotamers is independent of the orientation about $\omega$. For example, in *gt* of **1**, ~53% of the $\theta$ rotamers is *g*−, ~17% is trans, and ~29% is *g*+; virtually identical relative populations are found in *gg* (Table 8). Similar results were obtained for **2**, suggesting that anomeric configuration exerts little or no effect on correlated conformations about $\omega$ and $\theta$ in the *gluco* configuration.

The distribution of $\omega$ rotamers predicted from single (i.e., noncorrelated) analyses is in excellent agreement with that predicted from the correlated analyses (Tables 7 and 8).

**b. Distribution of ($\omega$,$\theta$) Rotamers in 3/4.** Overall weighted rms errors for $A_1-A_3$ regression analyses performed on **3** range from 0.6 to 0.7 Hz, while slightly greater errors were found for **4** (0.7−0.9 Hz). Among all regression analyses, those performed assuming nonperfectly staggered $\omega$ and $\theta$ (i.e., $A_1$ and $A_3$) yielded smaller overall rms errors than those based on perfectly staggered rotamers.

As observed for **1**/**2**, the populations of $\omega$ and $\theta$ rotamers predicted from the $A_1-A_3$ analyses were similar (Table 7). Thus, in **3**/**4**, *gt* predominates (~70%), followed by *tg* (~30%). Virtually no *gg* rotamer was observed. No effect of anomeric configuration on $\omega$ rotamer populations was found in **3**/**4**, in contrast to results obtained on **1**/**2**. With regard to $\theta$, the *g*+, *g*− and trans rotamers are roughly equally populated (Table 7). Unlike **1**/**2**, the *distribution* of $\theta$ rotamers in **3**/**4** depends on the orientation about $\omega$. In the *gt* form of both **3**/**4**, *g*−, *g*+ and trans $\theta$ rotamers are roughly equally populated, whereas in *tg*, *g*− predominates, followed by *g*+ and trans (Table 8). The effect appears to be caused by a significant reduction in the trans conformation about $\theta$ in *tg* compared to *gt* in both **3**/**4**.

As found for **1**/**2**, the distribution of $\omega$ rotamers predicted from single (i.e., noncorrelated) analyses was in excellent agreement with that predicted from the correlated analyses (Tables 7 and 8).

## Conclusions

Numerous experimental and theoretical determinations of hydroxymethyl group conformation and dynamics have been reported in aldohexopyranosyl rings.[38] An early X-ray crystallographic study[38a] showed that $\omega$ populations change significantly when O4 changes from equatorial (in *gluco*; *gt*/*gg*/*tg* ≈ 40:60:0) to axial (in *galacto*; *gt*/*gg*/*tg* ≈ 58:8:34). NMR studies[38] have yielded estimates of the *gt* (30−55% for *gluco*, 55−78% for *galacto*), *gg* (45−70% for *gluco*, 10−25% for *galacto*), and *tg* (−25−25% for *gluco*, 2−30% for *galacto*) rotamer populations. The literature has been reviewed recently by Bock and Duus.[39] Despite extensive work, however, the NMR approaches to this problem have remained constant for decades. Virtually all of the available analyses rely on two $^3J_{HCCH}$, and only more recently on two $^3J_{CCCH}$. Furthermore, rotamer populations based solely on $^3J_{HH}$ are highly protocol-dependent, resulting in significant anomalies (note the broad range of reported population percentages above). In addition, $^3J_{HH}$ analyses have frequently yielded substantial negative *tg* populations in *gluco* sugars.[39] The latter problem is attributed in part to the use of inaccurate torsion angles in the limiting staggered rotamers, which leads to errors in the estimates of the limiting *J*-values.

Tvaroska et al.[32] recently determined the populations of *gt*, *gg*, and *tg* forms in **1**−**4** and related compounds in $^2H_2O$ and methanol using either $^3J_{H5,H6R/S}$ or $^3J_{C4,H6R/S}$. In this work, substantial differences were reported in the populations derived from both parameters for nearly all compounds, with a maximal uncertainty of 46% for *gg* rotamers in methyl 6-*O*-methyl-α-D-glucopyranoside.

New structural constraints to assess $CH_2OH$ group conformation in saccharides based on multiple, redundant *J*-couplings have been described in this report. Using theoretical and experimental methods, equations were developed to correlate the magnitudes and signs of 12 scalar couplings with $CH_2OH$ conformation. Importantly, some of these couplings display a dependence not only on $\omega$ but also on $\theta$, in some cases exhibiting a greater dependence on the latter than on the former. These second-order dependencies serve as indirect probes of C−O bond conformation in solution that do not depend on direct observation/detection of the exchangeable hydroxyl proton. More importantly, use of these equations allows assessments of correlated conformation about $\omega$ and $\theta$.

Several key observations were made while developing these new constraints, which are summarized as follows:

(a) DFT provides a nearly quantitative tool to calculate $J_{HH}$, $J_{CH}$, and $J_{CC}$ values in saccharides, judging from comparisons of calculated and experimental couplings in conformationally constrained systems. In this work, unscaled couplings were employed. The theory appears sufficiently robust to yield accurate couplings in terms of magnitude and sign, thus obviating the need to impose empirical scaling adjustments common to studies of this type.[41] The small deviations (<10%) are likely caused by neglected conformational factors, neglect of non-Fermi contact contributions, and/or solvation effects. Further work is needed to establish the relative importance of these factors in order to incorporate further corrections or refinements to the methodology.

(41) (a) Houseknecht, J. B.; McCarren, P. R.; Lowary, T. L.; Hadad, C. M. *J. Am. Chem. Soc.* **2001**, *123*, 8811−8824. (b) Houseknecht, J. B.; Lowary, T. L.; Hadad, C. M. *J. Phys. Chem. A* **2003**, *107*, 372−378.

(b) $^2J_{CCH}$ display a large sensitivity to $\omega$ if their signs are taken into account. Importantly, prior suggestions that $^2J_{CH}$ values are sensitive to C−O torsions have been confirmed and quantified. This effect appears more significant for C−O torsions involving the carbon bearing the coupled proton than for C−O torsions involving the coupled carbon.

(c) Different Karplus equations apply to the interpretation of $^3J_{C4,H6R}$ and $^3J_{C4,H6S}$, in contrast to the prior generalized treatment of these couplings.[31] This behavior mimics that observed for $^3J_{H5,H6R}$ and $^3J_{H5,H6S}$.[6]

(d) $^1J_{C5,C6}$ depends on both $\omega$ and $\theta$, as anticipated based on previous studies of $^1J_{CC}$ in ethylene glycol.[34] The present work defines a quantitative relationship between both torsions and $^1J_{CC}$ magnitude.

(e) $^3J_{C1,C6}$ and $^3J_{C3,C6}$ may be useful additional experimental constraints on $\omega$. This sensitivity stems from the effect of terminal electronegative substituent orientation on the Karplus dependencies of $^3J_{CCCC}$ and $^3J_{COCC}$.[1]

(f) Given the simplicity of the present systems compared to ethylene glycol, greater insight into the stereoelectronic effects of oxygen lone pairs on saccharide bond lengths, and concomitant effects on *J*-couplings, especially $^1J_{CC}$, was obtained. In addition to their use in conformational analysis, *J*-couplings provide a means to indirectly evaluate saccharide electronic and stereoelectronic structure, both of which dictate their chemical and biological functions.

Nine independent $\omega/\theta$ rotamers in **1**−**4** were assumed in the present treatment, and their populations were calculated from the multilinear regression of 12 *J*-couplings. The data show that $\theta$ rotamer distribution may be affected by $\omega$ in O6-unsubstituted molecules. However, skewing in favor of specific $\theta$ rotamers is not large, suggesting that H-bonding solvation scaffolds, if present, do not freeze C−O rotamers completely. It will be important to test these conclusions via studies of $^3J_{HCOH}$[40] and $^3J_{CCOH}$,[42] which may provide complementary information on C−O conformation in aqueous solution.

The present study focused on free $CH_2OH$ groups in four methyl aldohexopyranosides (**1**−**4**) to establish new *J*-coupling/structure correlations in simple, well understood systems. While the application of these correlations to unsubstituted $CH_2OH$ groups has practical benefits (e.g., in oligosaccharides where intramolecular H-bonding may influence $\omega$ and/or $\theta$), more significant applications are expected in compounds such as 1,6-linked oligosaccharides containing substituted $CH_2OH$ groups. These linkages are characterized by three torsions and can display significant conformational flexibility. Recent studies have addressed the concerted use of $^2J_{COC}$, $^3J_{COCH}$, and $^3J_{COCC}$ across glycosidic linkages to assess rotamer populations about $\phi$ and $\psi$.[1,2] In 1,6-linkages, however, *$\psi$ and $\theta$ are redundant*, and thus a significant number of redundant *J*-couplings can now be brought to bear on this torsion *from both sides of the glycosidic linkage*. Furthermore, *correlated conformation about $\omega$ and $\theta/\psi$ can be investigated*, thus providing more detailed information on linkage flexibility.

Access to multiple *J*-couplings sensitive to $CH_2OH$ conformation render recently described theoretical approaches to assigning $CH_2OH$ conformation applicable to carbohydrate systems. The CUPID method[43] allows for calculations of a continuous rotamer distribution from NMR data provided that six conformationally sensitive parameters are available to determine a Fourier expansion of the order three. The maximum entropy method[30d] can be applied more effectively through access to an increased number of experimental NMR constraints.

The present findings have implications not only for studies of $\omega$ and $\theta$ in exocyclic hydroxymethyl groups in oligosaccharides but also for related studies in oligonucleotides. However, the equations reported herein were derived for pyranosyl rings. Further work is needed to determine whether modifications are required to treat furanosyl rings.

Finally, it should be noted that exocyclic $CH_2OH$ conformation cannot be assessed via $^3J_{HH}$ in some molecules. For example, $^3J_{HH}$ values are unavailable to study conformation about the C1−C2 bond in 2-ketohexoses such as D-fructose. In these cases, the additional *J*-coupling constraints reported herein could be advantageous.

**Acknowledgment.** This work was supported by a postdoctoral fellowship from the Knut och Alice Wallenberg stiftelse (Stockholm, Sweden) (to R.S.) and grants from Omicron Biochemicals, Inc. of South Bend, IN and the National Institutes of Health (GM59239) (to A.S.). The Notre Dame Radiation Laboratory is supported by the Office of Basic Energy Sciences of the United States Department of Energy. This is Document No. NDRL-4498 from the Notre Dame Radiation Laboratory.

**Supporting Information Available:** Short discussion of the effect of $\omega$ on C5−C6, C6,H6*R*/*S*, C5−O5 and C6−O6 bond lengths and $^1J_{C5,C6}$ in **5** (Figures S1 and S2); Figure S3 (Effect of $\omega$ on $^3J_{C1,C6}$ and $^3J_{C3,C6}$ in **5**); Figure S4 ($^1$H NMR spectrum of **4**); Figure S5 ($^{13}$C NMR spectrum of **3**); Tables S1−S3 (Calculated Scalar Couplings in **6** and **7**; Torsion Angles, $\omega$ and $\theta$, and Calculated $^3J_{CH}$ Values in **5**; Torsion Angles, $\omega$ and $\theta$, and Calculated $^1J_{CC}$ and $^2J_{CC}$ Values in **5**); Tables S4−S11 containing detailed results of single $\omega$ population analyses, and correlated $\omega/\theta$ population analyses in **1**−**4**. This material is available free of charge via the Internet at http://pubs.acs.org.

JA0306718

(42) Dais, P.; Perlin, A. S. *Can. J. Chem.* **1982**, *60*, 1648−1656.

(43) (a) Dzakula, Z.; Westler, W. M.; Edison, A. S.; Markley, J. L. *J. Am. Chem. Soc.* **1992**, *114*, 4, 6195−6199. (b) Dzakula, Z.; Edison, A. S.; Westler, W. M.; Markley, J. L. *J. Am. Chem. Soc.* **1992**, *114*, 6200−6207.

(44) (a) Serianni, A. S.; Bondo, P. B.; Zajicek, J. *J. Magn. Reson.* **1996**, *112B*, 69−74. (b) Zhao, S.; Bondo, G.; Zajicek, J.; Serianni, A. S. *Carbohydr. Res.* **1998**, *309*, 145−152.